Author Manuscript

Author Manuscript

Author Manuscript

Author Manuscript

HHS Public Access

Author manuscript

Sens Actuators A Phys. Author manuscript; available in PMC 2021 December 21.

Published in final edited form as:

Sens Actuators A Phys. 2021 December 01; 332(Pt 2): . doi:10.1016/j.sna.2021.112925.

Acoustics at the nanoscale (nanoacoustics): A comprehensive literature review.:

Part II: Nanoacoustics for biomedical imaging and therapy

Chang Peng[a], **Mengyue Chen**[a], **James B. Spicer**[b], **Xiaoning Jiang**[a,*]

[a]Department of Mechanical and Aerospace Engineering, North Carolina State University, Raleigh, NC 27695, USA

[b]Department of Materials Science and Engineering, The Johns Hopkins University, 3400 North Charles Street, Baltimore, MD 21218, USA

Abstract

In the past decade, acoustics at the nanoscale (i.e., nanoacoustics) has evolved rapidly with continuous and substantial expansion of capabilities and refinement of techniques. Motivated by research innovations in the last decade, for the first time, recent advancements of acoustics-associated nanomaterials/nanostructures and nanodevices for different applications are outlined in this comprehensive review, which is written in two parts. As part II of this two-part review, this paper concentrates on nanoacoustics in biomedical imaging and therapy applications, including molecular ultrasound imaging, photoacoustic imaging, ultrasound-mediated drug delivery and therapy, and photoacoustic drug delivery and therapy. Firstly, the recent developments of nanosized ultrasound and photoacoustic contrast agents as well as their various imaging applications are examined. Secondly, different types of nanomaterials/nanostructures as nanocarriers for ultrasound and photoacoustic therapies are discussed. Finally, a discussion of challenges and future research directions are provided for nanoacoustics in medical imaging and therapy.

Keywords

acoustics; nanotechnology; nanoacoustics; nanomaterials; biomedical applications; imaging; therapy; photoacoustics; laser ultrasound; sonothrombolysis

1. Introduction

The breakthroughs and advances in nanotechnology have provided various nanoscaled materials and devices with extraordinary characteristics for ultrasound investigations [1–5]. In many ways, the combination of nanotechnology with ultrasonics has revolutionized conventional approaches to use ultrasound. The emergence of different nanomaterials for the

*Corresponding author: xjiang5@ncsu.edu (Xiaoning Jiang).

Declaration of competing interest

Xiaoning Jiang has a financial interest in SonoVascular, Inc., who licensed an intravascular sonothrombolysis technology from North Carolina State University.

Author Manuscript Author Manuscript Author Manuscript Author Manuscript

support of diagnosis and treatment of various types of diseases has attracted increasingly more attention in past decades and has now become an important field of medical ultrasound. Motivated by the research innovations over the last decade, this paper, as part II of the two-part review of nanoacoustics, will concentrate on the nanoacoustics in biomedical imaging and therapy fields, including molecular ultrasound imaging, photoacoustic imaging, ultrasound-mediated drug delivery and therapy, and photoacoustic drug delivery and therapy. In the following sections, the review proceeds as follows: in Section 2, different kinds of nanomaterials and nanostructures to be adopted as contrast agents for biomolecular ultrasound imaging and photoacoustic imaging applications will be examined in detail. In Section 3, various types of nanomaterials and nanostructures to be utilized as nanocarriers for ultrasound-mediated drug delivery and therapy as well as photoacoustic drug delivery and therapy applications will be reviewed. The last section (Section 4) provides a summary and outlook for the nanoacoustic research in these fields.

2. Nanoacoustics for biomedical imaging

2.1. Molecular ultrasound imaging

Ultrasound imaging has been a popular medical imaging technique for decades, and is now the second most implemented imaging modality in clinical practice after X-ray radiography [6]. It has been widely utilized by physicians in diverse fields, including obstetrics and gynecology (OB-GYN), cardiology, radiology, as well as gastroenterology [7–11]. Compared with other imaging modalities, such as computed tomography (CT), magnetic resonance imaging (MRI), and photoacoustic (PA) imaging, ultrasound imaging shows the advantages, such as lack of ionizing radiation, high resolution, and low cost [12].

Due to the different acoustic properties of tissues and organs, ultrasound images can be generated while ultrasonic waves propagates through them [13–15]. The generation of images by ultrasound is based on the pulse-echo principle. A short pulse of ultrasonic waves generated by an ultrasonic transducer are transmitted into issues. A short time later, the echo pulses that are reflected from the tissue and organ interface are received by the same transducer or by a different transducer and are converted into electrical signals which are then utilized to generate a grayscale image displayed on the monitor, indicating the structure information. The depth of ultrasound image depends on the time between the transmitted pulse and the received echo. The echo amplitude is digitized and illustrated in the ultrasound image.

2.1.1. Contrast enhanced ultrasound imaging—Over the last few years, molecular ultrasound imaging, combining ultrasound technique with novel molecularly targeted contrast agents, has turned out to be a promising imaging technique for studying biological processes at the molecular level [16]. Microbubbles are by far the most commonly utilized ultrasound contrast agents (UCAs) owing to their widespread approval. They are composed of a gas core surrounded by a shell and usually 1–5 μm in size [17]. The gas core can generate a strong echogenic response which leads to a high contrast ratio on ultrasound images. The gas compositions usually applied in the gas core include air, nitrogen, and biologically-inert gases such as perfluoropropane, perfluorobutane, perfluorohexane, or

Author Manuscript Author Manuscript Author Manuscript Author Manuscript

sulfur hexafluoride (Figure 1a) [18]. The shell is utilized to prevent both gas leakage and stabilize microbubbles. The shell materials mainly consist of phospholipid, albumin and biocompatible polymers.

The bubble resonant frequency is the main parameter indicating the contrast efficiency. According to the small amplitude expansion of the Raleigh-Plesset equation, a nonlinear equation for describing oscillation of a spherical gas bubble in a liquid medium, the bubble resonant frequency is given by Equation 1 [20]:

$$f_0 = \frac{1}{2\pi R_0}\sqrt{\frac{1}{\rho_L}\left[3\gamma P_0 + \frac{2(3\gamma-1)\sigma}{R_0} + \frac{4\chi}{R_0}\right]} \quad (1)$$

Where f_0 denotes the resonant frequency of a bubble, R_0 denotes the bubble radius, ρ_L denotes the density of surrounding liquid, γ denotes ratio of the specific heat of the gas inside the bubble, P_0 denotes the liquid pressure, σ denotes the surface tension at the gas-liquid interface, and χ denotes the shell elasticity.

While there has been numerous diagnostic applications in clinical radiology and cardiology using microbubbles combined with ultrasound, microbubbles cannot extravasate into the tissue and therefore cannot be utilized as extravascular contrast agents due to their relatively large size. In order to exploring the extravascular space, smaller, submicron UCAs have showed widespread interest, especially in the field of oncology [12]. Submicron UCAs are so small that can extravasate through the leaky cancerous vasculature into interstitium, which is promising for the clinical applications such as highlighting lesion locations and delivering a payload of drugs [21–23]. Nevertheless, according to Equation 1, the bubble size is inversely related with the bubble resonant frequency. The higher ultrasound frequency is required for acoustic signal detection in case of the smaller bubble size. Likewise, improving shell stiffness will also lead to a higher bubble resonant frequency.

In addition, reducing the bubble size into nanoscale will not only lower its echogenicity in ultrasound examination, but decrease its stability in solution as well. The bubble stability is closely related with the Laplace pressure [24], as given by Equation 2:

$$\Delta P = (P_b - P_a) = \frac{2\sigma}{R} \quad (2)$$

Where ΔP is the Laplace pressure, P_b is the total pressure in bubble, P_a is the ambient pressure outside obubble. Reducing the bubble radius (R) will result in an increase of the Laplace pressure (ΔP), which will decrease the bubble stability. In order to increase the nanobubble stability, surfactants or lipids are usually bonded to the surface of nanobubbles to serve as elastic shells counteracting the effect of surface tension. Moreover, the choice of the gas core in a nanobubble is crucial to its stability as well. The application of a perfluorocarbon gas core rather than gas compositions commonly used in microbubbles, such as air, nitrogen and sulfur hexafluoride, can largely reduce the bubble dissolution time owing to its low solubility in the blood (Figure 1b).

Author Manuscript Author Manuscript Author Manuscript Author Manuscript

2.1.2. Organic and inorganic nanosized UCAs—A variety of nanosized UCAs have been developed and reported by many researchers, which offers a paradigm shift of contrast enhanced ultrasound in both medical diagnostics and therapeutics [25–28]. Such agents are chemical-based agents that are produced by organic (Figure 2a–c) or inorganic materials (Figure 2d) [29]. The applications of these agents as ultrasound molecular imaging contrast agents will be examined, while many of them can also be utilized theranostic agents that provide the combination of diagnostics and therapeutics in a single nanoscale agent. The reported organic and inorganic nanosized UCAs and their applications are presented in Table 1 and Table 2, respectively [29].

2.1.3. Biogenic gas vesicles—Besides chemical-based agents, genetically engineered protein-shelled nanoparticles, gas vesicles (GVs), have also illustrated remarkable imaging performance as molecular ultrasound contrast agents. GVs are hollow proteinaceous nanostructures with cylinder or spindle shapes, which are composed of a 2 nm-thick protein shell that encapsulates a hollow interior normally filled with air (Figure 3a–b) [70]. The shell of GVs has a highly hydrophobic inner surface, thereby water cannot pass through it and water vapor cannot condense inside [71]. However, ambient gases are able to freely diffuse into and out of GVs. In 2014, Shapiro et al. [72] first found that purified GVs from a kind of photosynthetic bacteria which were used to regulate buoyancy could scatter ultrasound waves and thus produce ultrasound contrast.

Because GVs are filled with gas, it was assumed that GVs could act as nanoscale contrast agents for ultrasound imaging. This hypothesis was then verified by using GVs purified from *Anabaena flos-aquae* and *halobacteria NRC-1* and ultrasound imaging in a gel phantom at 4.8, 8.6 and 17 MHz [72]. Following this pioneering finding, many studies about using GVs as biomolecular contrast agents have been conducted, such as exploring their acoustic properties [73,74], engineering them through genetic and biochemical modulations [75,76], investigating the in vivo biodistribution as molecular contrast agents [77], using them as biomolecular tool for deep tissue imaging [78–80], imaging of microorganisms inside living animals (Figure 3c–f) [81], as well as more dedicated imaging of generic expression in mammalian cells [82].

2.2. Photoacoustic (PA) imaging

2.2.1. Principle of PA imaging—Photoacoustic (PA) imaging (also referred to as optoacoustic imaging) is an emerging multiscale functional, anatomical, and molecular imaging modality, having demonstrated great promise in preclinical researches and clinical applications [84]. PA imaging is based on photoacoustic effect that light absorbed by tissues is used to excite ultrasonic waves via thermoelastic expansion. In PA imaging, nanosecond duration laser pulse is delivered into the animal tissues (Figure 4). The absorption of short laser pulses by endogenous chromophores (such as hemoglobin and melanin) or exogenous contrast agents (such as small molecule dyes and carbon nanoparticles) is converted into thermal energy that results in transient thermoelastic expansion to generate acoustic waves in 3D space. The ultrasound waves can then be detected with an ultrasonic transducer or a transducer array surrounding the tissue or animal body. The detected ultrasonic waves are analyzed to reconstruct a photoacoustic image of tissue optical absorption [85].

Author Manuscript Author Manuscript Author Manuscript Author Manuscript

A PA imaging system mainly consists of an optical source for short laser pulse generation, an ultrasonic transducer array for acoustic wave detection, and a data acquisition (DAQ) system [86]. The pulse repetition frequency of the laser pulse and the time for ultrasonic signals detection are two major factors determining the PA imaging frame rate. Combining advantages from both optical and ultrasound imaging, PA imaging offers unique advantages over existing imaging modalities. First of all, PA imaging is free of ionizing radiation and noninvasive, thus it can be safely used in vivo. Secondly, it has higher resolution and deeper penetration depth (~ 4 cm in vivo and ~ 12 cm in vitro) compared to optical imaging techniques (~ 1 mm). Moreover, compared with other imaging modalities such as MRI and CT, PA imaging is much faster and less expensive. Other benefits include speckle free and label free [85,87–90]. With all these benefits, PA imaging has been found applications in diverse fields, including oncology, vascular biology, dermatology, neurology, ophthalmology, and cardiology [91–94].

2.2.2. Organic and inorganic nanosized contrast agents—Although PA imaging is able to penetrate deeper into tissue than other optical imaging methods, owing to the laser light scattering, the photoacoustic signal-to-noise ratio and light intensity attenuate exponentially with the increase of penetration depth, affecting the imaging contrast and resolution [85,95]. In order to enhance the PA imaging sensitivity and contrast, various oral or injectable chemicals, i.e., exogenous contrast agents, have been adopted to change the optical and acoustic properties of structures within the body [96]. Thus, the PA imaging contrast and resolution are reinforced with the assistance of exogenous contrast agents. In this section, the recent development of exogenous contrast agents that address biomedical applications and clinical practice will be examined. For the characteristics of endogenous chromophores and biomedical applications of PA imaging assisted with these chromophores, readers are referred to the references [97].

The exogenous PA contrast agents can be classified into organic and inorganic contrast agents according to their structures. A summary of recent reported PA organic and inorganic nanosized contrast agents is shown in Table 3. The highlights of different types of organic and inorganic nanosized contrast agents are presented in the following section. Various biomedical applications of PA imaging including bioimaging of tumors and biosensing of tumor microenvironments are summarized in Table 4.

(1) Organic contrast agents.: A typical representative of small organic molecules is cyanine-based dyes that are commonly utilized as PA imaging contrast agents as a result of their good photostability, high photoconversion efficiencies and negligible toxicity [115]. Kang et al. [102] reported a method to improve the PA response of indocyanine green (ICG), one of the commonly applied PA imaging agents, by encapsulating it in a porous silicon nanoparticle host. Because of the low thermal conductivity of the host, the PA generation efficiency of the composite structure was increased 17-fold compared with free ICG (Figure 5a). Liu et al. [114] developed a ratiometric photoacoustic nanoprobe consisting of liposome and $MeHg^+$-responsive NIR cyanine dye for $MeHg^+$ detection in living subjects (Figure 5b). It was found that in the presence of $MeHg^+$, the ratiometric photoacoustic signal was increased remarkably. Chen et al. [111] fabricated a nanoprobe composed of

Author Manuscript Author Manuscript Author Manuscript Author Manuscript

human serum albumin (HSA) and NIR dye (BPO_x and IR825) nanocomplexes for sensing tumor microenvironment pH using ratiometric photoacoustic imaging (Figure 5c). The tumor microenvironment pH could be detected by using the nanoprobe in combination of ratiometric photoacoustic imaging, which was very useful for regulating the proliferation of cancer cells.

Besides, owing to their strong optical absorption and high photostability, semiconducting polymer nanoparticles (SPNs) have also been commonly adopted [115]. By encapsulating PDI into micelle, a kind of amphiphilic molecule, Fan et al. [98] developed a highly efficient PA imaging contrast agent, micelle-enveloped PDI, for imaging of deep brain tumors (Figure 6a). Their studies found that the organic NPs illustrated strong PA absorption in the NIR range, and they could be utilized to detect brain tumors successfully in living mice. Following that, to diagnosis of early thrombus and monitoring thrombolysis, Cui et al. [105] developed cyclic Arg-Gly-Asp (cRGD) peptide modified PDI (cRGD-PDI) NPs as PA agents. The cRGD-PDI NPs showed strong PA imaging contrast and provided 4-folder greater PA intensity of early thrombus than the control group in a living mouse (Figure 6b). In another study, in order to achieve the combined PA and US imaging, Tang et al. [116] fabricated an organic semiconducting nanodroplet consisting of a PDI shell, a liquid perfluoropentane core and photosensitizers of $ZnF_{16}P_c$ molecules at the interface of the core-shell as PA and US dual-contrast agents (Figure 6c). The nanodroplets illustrated a high tumor accumulation in a living mouse due to their nanoscale size. Under a 671 nm laser irradiation, the nanodroplets could be effectively applied for dual-modal PA and US imaging-guided photothermal and photodynamic therapy.

(2) Inorganic contrast agents.: Metallic nanomaterials, especially gold nanoparticles (AuNPs), can achieve strong optical absorption via the localized surface plasmon resonance (LSPR) [85]. By synthesizing AuNPs with different morphologies, their optical absorption properties can be maximized in the NIR region. Other notable advantages of AuNPs include their biocompatibility, high photothermal conversion efficiency, and good chemical inertness [117,118]. To date, different types of AuNPs have been reported including nanospheres [119–121], nanorods [122–125], nanoprisms [126–128], nanocages [129–131], nanostars [132–134], nanoplates [106,135,136], nanodisks [137–139], nanoshells [64,140–142], nanovesicles [123], nanotripods [143], nanowreaths [144], nanoflowers [145,146], and bipyramids and rhombic dodecahedra [147], as shown in Figure 7.

Besides the gold nanocrystals, gold nanocrystal assemblies also show outstanding optical absorption properties in the NIR region. Bai et al. [151] fabricated a multifunctional nanocomposite combining imaging (PA imaging and MRI) and therapeutic functions for cancer cells imaging and photothermal therapy, which was composed of hollow gold nanospheres as cores and superparamagnetic iron oxide NPs as satellites. Song et al. [152] developed a plasmonic vesicular nanostructure comprising of amphiphilic gold nanocrystals with polymer brush coatings. The nanocrystals imparted their remarkable properties to the assembly, and the strong interparticle plasmonic coupling caused collective properties different from those of the constitutive units. In another work, Deng et al. [153] developed a theranostic agent composed of comb-like amphipathic polymer template and DOX@gold nanomicelles for dual-modal imaging (CT and PA) and the combination of

Author Manuscript Author Manuscript Author Manuscript Author Manuscript

chemotherapy and photothermal therapy. Their studies in a mouse model demonstrated that the nanomicelles could be effectively used to detect tumors for CT and PA imaging simultaneously. Carbon-based nanomaterials mainly consisting of CNTs [154–156] and graphene-based nanomaterials [157–161], have been widely adopted as contrast agents in PA imaging as well (Figure 8a). The major advantages of carbon-based nanomaterials are their broad absorbance band ranging from UV to NIR region as well as ease to integrate with various materials or compounds for multiple functions. De La Zerda et al. [162] synthesized a PA contrast agent based on SWNT conjugated with RGD peptides for PA imaging of tumors. According to the tumor detection in a living mouse, the PA signal of the tumor in the mouse injected with the contrast agents was eight times stronger than that of the control group. Kim et al. [163] reported gold-plated carbon nanotubes as contrast agents for PA imaging, which were composed of shortened SWNT core coated by a thin layer of gold. This novel hybrid plasmonic contrast agent, combined the advantages of gold and CNTs, presented a unique set of features. Song et al. [164] proposed a PA contrast agent fabricated by carbon nanotube ring (CNTR) template and AuNPs coating for imaging-guided cancer therapy (Figure 8b). Compared with CNTR and CNTR@AuNS, the CNTR@AuNP illustrated much stronger Raman and optical signals. Moon et al. [165] developed a PA imaging contrast agent rGO-AuNRs using an optically absorbing material rGO coated with gold nanorods (Figure 8c). The rGO-AuNRs demonstrated greatly enhanced PA signal intensity and photothermal efficiency, which was a promising nanomaterial for sensitive disease diagnosis and photothermal therapy. In addition, Song et al. [166] fabricated a carbon-metal hybrid rGO-loaded plasmonic gold nanorod vesicle for dual chemo-photothermal therapy. The rGO was conjugated with DOX and the rGO-DOX conjugation was encapsulated in the AuNRVe to avoid direct interaction with the physiological environment.

3. Nanoacoustics for medical therapy

3.1. Ultrasonic drug delivery

Apart from diagnostic applications of ultrasound, therapeutic applications of ultrasound, such as ultrasound-mediated drug/gene delivery, has become an emerging topic of expanding interests. Starting from the mid-90s, many studies have reported that the exposure to ultrasound can temporarily enhance the cell membrane permeability (i.e., sonoporation), thus creating a physical channel for delivery of cell-impermeable drugs (Figure 9) [168]. The main benefit of delivery of therapeutics using ultrasound is that the drug delivery and release is spatially and temporally controlled in the target region, thus lowering the dosage use and the adverse side effects [169,170]. Different therapeutics including small-molecule drugs, protein drugs, peptide drugs, and genetic drugs have been reported to be successfully delivered with the assistance of ultrasound waves [171–176].

While microbubbles have been proved to be reliable tools for ultrasound-mediated therapeutic delivery, the key limitation of microbubbles is that the size of microbubbles is too large to penetrate into tumor tissues, thereby only confined their applications in blood circulation and cannot be effectively utilized for cancer therapy [23]. Various techniques have been devised for the use of nanosized bubbles/particles for delivery of therapeutics to

Author Manuscript Author Manuscript Author Manuscript Author Manuscript

targeted tissues [178]. Nanobubbles/particles, acted as delivery carriers, are able to deliver drugs precisely to the target tissues while maintaining efficiency. Moreover, combined with the visual and noninvasive features of ultrasound, the motion of drug nanocarriers can be tracked and the release of drugs from nanocarriers can be controlled by the ultrasound irradiation [179,180]. For all these reasons, the development of safe and efficient novel ultrasound-responsive therapeutic nanocarriers could greatly impact therapy strategies.

3.1.1. Nanocarriers for ultrasonic drug delivery—

Recently, there have been various nanomaterials served as nanocarriers for delivery of anticancer drugs to tumor tissues [181–183], delivery of thrombolytics to break up or dissolve blood clots [184–186], delivery gene to target tissues [187–190], as well as delivery insulin to regulate blood glucose level [191,192] (Figure 10). The recent development of different types of nanocarriers for ultrasonic drug delivery are highlighted in this section.

(1) Liposomes.: Liposomes, typically with a diameter of 100–200 nm, are composed of an aqueous core surrounded by a self-assembled lipid bilayer membrane. Due to their excellent biocompatibility and versatility, liposomes has become one of the most widely utilized nanocarriers for ultrasound-mediated drug delivery [194]. Marxer et al. [195] developed a long-circulating drug nanocarrier with three different lipid formulations for ultrasound-enhanced drug delivery. The physico-chemical properties of the developed lipid dispersions were compared with a commercially available contrast agent, which demonstrated adjustable properties including circulation stability, biocompatibility, and ultrasound reflectivity. In another study, Becker et al. [196] compared the sonothrombolytic efficacy of the three nanoscaled lipid formulations with the commercially available contrast agent for human blood clot under diagnostic ultrasound. Their results illustrated that the nanoscaled formulation of DSPC/PEG40S had the most significant clot weight reduction under the irradiation of ultrasound at 1.4 MHz, even without thrombolytic drugs. Lattin et al. [197] reported an echogenic liposome that can release drugs from liposomes under ultrasound excitation. The developed liposomal drug nanocarrier was called an eLiposome (liposomes containing emulsion droplets), formed by using a lipid sheet folding technique. The eLiposome had an overall diameter of 800 nm and contained emulsion droplets 100–150 nm and 470 nm, respectively. Under ultrasound excitation, vapor phase was formed and expanded from the droplets, which would disrupt the liposomal membrane and lead to local drug release.

(2) Micelle.: Micelle is typically spherical in shape, which is formed by a series of amphiphilic molecules that have a natural tendency to clump together. The hydrophobic drugs can be segregated in the hydrophobic core of micelle until they are released. Diaz de la Rosa et al. [198] investigated anticancer drug DOX release behavior from Pluronic P105 unstabilized and stabilized micelles. The in vitro experiments found that the drug release from unstabilized as well as stabilized micelles at ultrasound frequency < 90 kHz, while no drug was released from the micelles at ~500 kHz. This was mainly attributed to the different dynamics of oscillating bubbles under the different ultrasound excitations. Husseini et al. [199] fabricated DOX encapsulated Pluronic P105 micelles with a folic acid moiety to enhance the tumor cells targeting. They found that the percentage of

Author Manuscript Author Manuscript Author Manuscript Author Manuscript

drug release was improved with the rise of ultrasound power intensity under 70 kHz excitation. The maximum amount of DOX release was 14%, which was measured at an ultrasound intensity of 5.4 W/cm^2. Wu et al. [200] developed anticancer drug curcumin (Cur) encapsulated pluronic P123/F127 mixed micelles for site-specific sonochemotherapy. Under 1 MHz focused ultrasound excitation, the Cur-loaded micelles demonstrated tumor-targeting deposition, resulting from the ultrasound sonoporation. Moreover, the ultrasound-triggered Cur release from the Cur-loaded micelles was highly dependent on the ultrasound intensity.

(3) Polymeric nanoparticles.: Polymeric nanoparticles mainly consist of nanocapsules, nanospheres, and polymersomes, which demonstrate the properties of enhanced encapsulation and controlled release of therapeutics [201]. Nestor et al. [202] fabricated air-filled nanocapsules with a biodegradable polymeric shell for tumor detection. The nanocapsules had a mean diameter of 370 nm and a spherical shape with smooth surfaces as well as a capsular morphology. The polymeric shell could potentially entrap drugs inside it, which made this kind of structure promising for theranostics agents. Yang et al. [203] reported a biodegradable nanocapsule that was filled with perfluorohexane and had the DOX-loaded PMAA as wall for achieving the ultrasound imaging and drug delivery functions. The developed nanocapsules could easily enter the tumor tissues due to their small and uniform size. Moreover, the filled perfluorohexane could be easily vaporized via ultrasound excitation, thus enhancing ultrasound imaging signals and ensuring imaging-guided drug delivery. Chen and Du [204] developed polymer vesicles that responded to both ultrasound and pH stimuli for drug entrapment and release. The size of the vesicles would become smaller under either ultrasound excitation or pH decrease. The encapsulated anticancer drugs could reach controllable release when exposed to ultrasound irradiation or pH variation.

(4) Nanobubbles.: Nanobubbles are commonly adopted as theranostic agents due to their great imaging ability. Cavalli et al. [205] developed DNA-loaded chitosan nanobubbles which were composed of a perfluoropentane core and a chitosan shell as ultrasound-triggered gene delivery system. The plasmid DNA was loaded onto the chitosan shell, which was expected to have long circulation time and accumulate into tumor tissues easily. Based on the in vitro experiments, while in the absence of ultrasound, the nanobubble-bound plasmid DNA was not released at all, after one minute of 2.5 MHz ultrasound excitation, the release of plasmid DNA occurred. Yin et al. [206] developed siRNA-loaded nanobubbles which were fabricated by the negatively charged gas-cored liposomes and positively charged siRNA micelles for tumor treatment. Under 1 MHz ultrasound irradiation, the siRNA micelles were effectively released from the nanobubbles in tumor tissue and delivered into cancer cells.

(5) Perfluorocarbons (PFCs).: Rapoport et al. [207] reported paclitaxel (PTX)-loaded perfluoropentane (PFP) nanoemulsions that could effectively accumulate in tumor tissue and transformed into microbubbles in sonication. The ultrasound imaging properties and therapeutic efficacy of the nanoemulsions were experimentally verified in a mouse model. After injection of the drug-loaded nanoemulsions, tumors were significantly regressed after1

Author Manuscript Author Manuscript Author Manuscript Author Manuscript

MHz ultrasound irradiation. In another study, Thakkar et al. [208] explored the effect of ultrasound irradiation on the penetration of drug-loaded nanoemulsions through vascular walls. Mouse carotid arteries were utilized as a blood vessel model. They found that under 1 MHz irradiation, the permeability of the arteries to the nanoemulsions was much more pronounced by using continuous ultrasound wave than that of pulsed ultrasound.

(6) Quantum dot.: Based on the fact that ultrasound irradiation can enhance cell membrane permeability (sonoporation), Thein et al. [187] developed an ultrasonic micro-transducer array for cellular level controllable sonoporation that accelerates delivery of drugs or gene therapeutics to cells (Figure 11). The developed transducer array was composed of 3 × 3 arrays of PMN-PT transducers (each area 25 μm × 25 μm) with a central frequency of 30 MHz and lateral resolution of 18 μm for site-specific sonoporation. CdSe/ZnS quantum dots were utilized as nanocarriers to quantitatively evaluate the sonoporation degree of the human melanoma cells seeded on the surface of the transducer array. It was found that the cell membrane wound size and cellular uptake of quantum dots were increased linearly with the rise of ultrasound irradiation pressure.

Besides the nanocarriers reviewed above, other inorganic materials including mesoporous silica nanoparticles [209–214], Au nanocages [215–217], magnetic nanoparticles [218–220], and carbon-based nanovehicles [69,221–224] have also been reported by researchers to be utilized as nanocarriers for ultrasound-mediated drug delivery.

3.2. Ultrasound therapy

3.2.1. Ultrasound-triggered therapy—Ultrasound has long been employed in medicine for the treatment of many different pathologies, such as ultrasound-assisted liposuction, lithotripsy for kidney stone, and accelerating wound healing, mainly attributed to its advantages of safety to human tissues, low cost and deep tissue penetration capability [225]. Recently, high-intensity focused ultrasound (HIFU) has been served as a new noninvasive treatment technique for thermal ablation of local tumors [226]. Sonodynamic therapy (SDT) that is based on low-intensity ultrasound and chemotherapeutic agents (known as sonosensitizer) has been reported by researchers to noninvasively eradiate solid tumors due to the ultrasound-induced cytotoxic effects [227]. Compared with the current major therapeutic techniques including chemotherapy and gene and cell therapy, ultrasound-triggered therapy is able to focalize at target tissues and reduce biotoxicity. In addition, better treatment could be achieved while combining the ultrasound method with conventional therapies [228].

Over the past few decades, the rapid development of nanomaterials and nanostructures not only advances ultrasound imaging by providing nanosized contrast agents with outstanding properties, but also accelerates ultrasound therapy with greatly enhanced therapeutic efficiency owing to their unique physiochemical properties, such as surface features, geometry, porosity, and composition [229]. Different nanoparticles can also potentially combine several imaging modalities and therapeutic functions into one nanoplatform to be utilized as multifunctional theranostic agents for imaging-guided synergistic therapy. Miscellaneous nanoparticles including organic nanomaterials and inorganic nanomaterials

Author Manuscript Author Manuscript Author Manuscript Author Manuscript

have been adopted in studies for treatment various diseases such as tumors, cardiovascular diseases, and central nervous system diseases [228].

While this section is focused on nanomaterials and nanostructures for ultrasound-triggered therapy applications, many recent published review articles have already covered this topic, especially the review about nanoparticles for ultrasound-triggered cancer therapy. Considering that several comprehensive reviews have summarized and discussed the emerging development of exploring organic and inorganic nanomaterials for ultrasound-triggered therapies, the same topic will not be reviewed again in this paper and the readers could refer to very recent reviews. Yang et al. [228] focused on the current applications of ultrasound-triggered therapy (2019). Zhou et al. [230] summarized the development of organic and inorganic nanoparticles for ultrasound-based cancer therapy (2020). Yang et al. [231] reviewed the recent advance of 2D nanomaterials for ultrasound-triggered cancer therapy (2020). Fan et al. [232] comprehensively examined nanotechnology-mediated synergistic cancer therapy (2017). Xu et al. [233] focused on different nanoparticles in sonodynamic therapy (2016). Unga et al. [234] reviewed nanosized agents for ultrasound-induced cancer immunotherapy (2014).

3.2.2. Nanoparticle-mediated sonothrombolysis—While blood clot, or thrombus, helps human body stop bleeding when a person gets hurt, blood clots forming in veins or arteries are dangerous to human health. When blood clots form inside a vein or artery (i.e., thrombosis), they will reduce the blood flow past the clot or even totally block the blood flow. If the thrombosis forms in the legs, it causes deep vein thrombosis; if it is formed in the lung, life-threatening pulmonary embolism will be occurred; if the blood clots block the blood supply to the brain, ischemic strokes will happen [235]. Thrombolysis, known as thrombolytic therapy, is a treatment to dissolve blood clots that have blocked veins or arteries and pose potentially serious or life-threatening complications. Sonothrombolysis is an emerging technique that employs ultrasound waves to break down blood clots in vessels. The widely accepted mechanisms of sonothrombolysis are ultrasound-induced stable and inertial cavitation, microstreaming, microjetting and increased diffusion of therapeutics into the clots due to acoustic radiation force [236]. Conventionally, sonothrombolysis is usually adopted in combination with thrombolytic agents, such as tissue plasminogen activator (tPA) or microbubbles. However, the application of tPA will carry the risk of systemic hemorrhage in patients, and the use of microbubble is showed to be slow for treatment (usually several hours) and less effective for aged clots [237,238].

Nanodroplets, a generally applied ultrasound contrast agent that has a diameter of 100–300 nm, has been shown to be effective for sonothrombolysis [239]. Compared with microbubbles, the advantages of nanodroplets include their longer circulation time in blood and deeper penetration into clots due to their smaller size. Recently, low-boiling-point (−2°C) lipid-shell perfluorocarbon phase-change nanodroplets were adopted by our group for sonothrombolysis based on the assumption that the smaller nanodroplets could permeate into a clot easier compared to microbubbles, thereby greater cavitation effects would be generated inside the clot and lysis rate would be improved [240]. The efficiency of the nanodroplets for sonothrombolysis was compared with that of microbubble-mediated sonothrombolysis. Under the same ultrasound excitation conditions (I_{SPTA} 0.384 W/cm^2,

Author Manuscript Author Manuscript Author Manuscript Author Manuscript

peak negative pressure 8.0 MPa), the nanodroplets-mediated treatment demonstrated a thrombolysis rate of 140% over the microbubble-mediated treatment. In another study, we conducted in-vitro study to compare the sonothrombolysis efficacy of nanodroplets on unretracted (< 24 hours old) and retracted (> 3 days old) blood blots with that of microbubbles [241]. The results illustrated that while the unretracted clot mass reduction was similar for both treatment conditions, the retracted clot mass reduction for the nanodroplet-mediated treatment was 1.6-fold over that of microbubble-mediated treatment. Under the treatment condition that tPA was combined with the nanodroplet-mediated sonothrombolysis for retracted clots, compared with control group (tPA + ultrasound), the nanodroplet-mediated sonothrombolysis with tPA illustrated greatly larger mass reduction (38% vs. 4%) [242].

Besides nanodroplets, magnetic microbubbles are also proved to be promising for sonothrombolysis. Magnetic microbubble (MMB), composed of a gas core and a shell of Fe_3O_4 nanoparticles, not only possesses the acoustic properties of a microbubble but also is sensitive to magnetic field excitation (Figure 12c) [243]. In our recent studies [244,245], MMBs were utilized in conjunction with an intravascular forward-looking ultrasound transducer (620 kHz) for MMBs-mediated sonothrombolysis (Figure 12a). We assumed that under a rotational magnetic field, the MMBs would be trapped and oscillated close to the target blood clot; the induced vortex-like microstreaming would enhance the cavitation effect generated by sonication. Based on our in vitro studies, the mass reduction of MMBs-mediated sonothrombolysis for unretracted and retracted clot was 1.4-fold over that of microbubble-mediated sonothrombolysis. To achieve precise and controllable delivery of thrombolytic drugs, Wang et al. [186] synthesized a nanoparticle-shelled magnetic microbubble (MMB-SiO_2-tPA) for realizing the magnetic targeting under a magnetic field and ultrasound-triggered tPA release due to the microstreaming. The microbubble was composed of an air core and a shell of nanoparticles consisting of Fe_3O_4 nanoparticles and tPA-containing mesoporous silica nanoparticles (Figure 12b). Under a low-intensity ultrasound excitation, both the penetration depth of tPA into clot and thrombolysis efficacy were improved. Compared with conventional injection of tPA (0.03 mg/kg), the thrombus mass in a mouse model was reduced by 67.5% using the MMB-SiO_2-tPA treatment.

3.3. Photoacoustic drug delivery and therapy

The PA imaging nanosized contrast agents have also been adopted by researchers as drug delivery vehicles since studies have found that the ultrasound irradiation generated by the PA effect could effectively accelerate the delivery and release of drugs in target tissues [246–248]. Furthermore, the local temperature rise of nanoparticles induced by the laser irradiation can cause thermal ablation and subsequent cancer cell death, i.e., photothermal therapy (PTT) [249]. The encapsulated drug release from nanocarriers can be promoted as well by the local heating generated in tumor tissues exposed to NIR laser irradiation [250,251].

3.3.1. Organic nanocarriers—Small molecular dyes and semiconducting polymer nanoparticles have also been commonly adopted for theranostic applications [252–258]. Gong et al. [259] reported a multifunctional nanomicelle fabricated by polyethylene

Author Manuscript Author Manuscript Author Manuscript Author Manuscript

glycol (PEG) coating and C18PMH conjugation for imaging-guided cancer therapy. Photosensitizer chlorin e6 (Ce6) was conjugated with C18PMH and photothermal agent IR825 was encapsulated into the nanomicelles. The resulted IR825@C18PMH-PEG-Ce6 nanomicelles could realize photoacoustic, fluorescence, and magnetic resonance triple modal imaging of tumors as well as combined photothermal and photodynamic therapy. Wang et al. [260] developed acid-switchable multifunctional nanomicelles for photothermal and chemotherapy of drug-resistant tumors. The nanomicelles were fabricated with PDPA-based polymeric matrix, which could cause dissociation of the nanostructures under acid condition. Photosensitizer Ce6 was conjugated with PDPA nanomicelles and DOX was loaded into the nanomicelles. The developed nanomicelles illustrated strong light absorption in the NIR region. Under NIR laser irradiation, the nanomicelles could effectively convert optical energy into local heat, which promoted PA imaging, drug penetration into tumor tissues as well as photothermal therapy. Cai et al. [261] synthesized a diketopyrrolopyrrole (DPP)-triphenylamine (TPA) organic nanoagent for PA imaging-guided photodynamic/photothermal cancer therapy (Figure 13a). TPA, a commonly used donor, was conjugated with the DPP core to form a donor-acceptor- donor (D-A-D) structure. The nanoagent illustrated excellent NIR absorption, high photothermal conversion efficiency, and outstanding synergetic therapeutic effect due to the enhanced D-A-D structure of the DPP-TPA conjugation. Recently, Zhang et al. [262] developed electron donor-acceptor (D-A) conjugated semiconducting polymer nanoparticles (PPor-PEG NPs) for PA imaging-guided photothermal cancer therapy. The developed NPs could induce strong PA signals in tumor site for a long time, indicating the potential to be a long-term contrast agent. Additionally, the NPs showed a remarkedly high photothermal conversion efficiency 62.3%, the highest reported value among the reported polymer NPs.

Fan et al. [263] developed a novel multimodal imaging nanoplatform using ultra-small (~ 7.5 nm) water-soluble melanin nanoparticles (MNPs) (Figure 13b). The NPs not only demonstrated good photoacoustic properties for PA imaging but also illustrated natural binding ability with metal ions (Fe^{3+} and $^{64}Cu^{2+}$) for MRI and PET. Following that, Zhang et al. [264] developed a melanin nanoparticle-based nanosystem for PA imaging-guided chemotherapy. Anticancer drug, sorafenib (SRF), was bonded with melanin NPs to form a water-soluble nanoplatform, demonstrating great biocompatibility and PA property for imaging-guided therapy. The developed SRF-MNPs exhibited excellent tumor therapeutic effect after injection into the tail-vein of a living mice. Di et al. [248] recently developed an alginate sphere microgel encapsulated with DOX and CIF-loaded PLGA nanoparticles as a platform for laser ultrasound controlled drug delivery (Figure 13c). The drug release from the microgels was triggered by the laser generated pulsed ultrasound excitation that was transmitted from a laser-generated focused ultrasound transducer, made with a carbon black/PDMS-photoacoustic lens. Once the microgels were excited by the ultrasound waves, cavitation effects were induced at the microgels, which accelerated the release of drugs from the nanoparticles.

3.3.2. Inorganic nanocarriers

(1) Metallic Nanomaterials.: Numerous investigations have been demonstrated that metallic nanomaterials, especially AuNPs, can act as drug carriers for PA imaging-guided

Author Manuscript Author Manuscript Author Manuscript Author Manuscript

chemotherapy and PTT [215,265–267]. For instance, Wilson et al. [268] developed a photoacoustic nanodroplet composed of a liquid PFC core containing AuNRs and a bovine serum albumin shell for combinational PA/ultrasound imaging and potential drug delivery. The nanodroplets could provide PA and ultrasound contrast improvement via the laser-induced vaporization of the liquid PFC nanodroplet and long duration thermal expansion of the AuNRs. Following that, Zhong et al. [269] designed a paclitaxel (PTX)-containing nanoparticle which was based on loading PTX and AuNRs into PFH nanodroplets for PA imaging-guided photothermal/chemo synergistic cancer therapy. Upon pulsed laser irradiation, the nanoparticle could be rapidly decomposed owing to PFH vaporization, resulting in fast drug release, which induced efficient apoptosis of cancer cells. Duan et al. [270] developed organic/inorganic nanohybrids consisting of AuNRs, quantum dots (QDs), mesoporous silica layer, and CD-PGEA for multimodal imaging-guided cancer therapy (Figure 14a). The AuNRs were integrated with QDs for combined PA, CT and fluorescent imaging. In addition, the high photothermal conversion efficiency of AuNRs facilitated them to be utilized for photothermal therapy. Antitumor drug, DOX, was loaded into the mesoporous structure of the silica layer and sealed by the CD-PGEA gatekeeper for both the drug and gene delivery.

Besides coating AuNRs with mesoporous silica, Huang et al. [271] synthesized a hollow-mesoporous nanocapsule consisting of AuNRs and iron oxide nanoparticles (IOs) for dual-modal PA imaging and MRI-guided synergistic photothermal/chemo tumor treatment (Figure 14b). The AuNRs was combined with the magnetic IOs via a yolk-shell structure, in which movable AuNRs were confined in the permeable IO nanoshells using silica templates. DOX was loaded into the mesoporous nanocapsule after the formation of the yolk-shell structure. Moon et al. [130] designed a new theranostic system composed of hollow nanostructured Au nanocages (AuNCs) and a phase-change material (PCM) (Figure 14c). Drugs were encapsulated into the PCM, and the PCM was functionalized as a gatekeeper to control the drug release corresponding to temperature rise. Two dyes used as drug models were loaded into the PCM. Under HIFU irradiation, the PCM was melted and escaped from the interior of AuNCs, simultaneously releasing the encapsulated drugs.

Prussian blue, a clinical medicine approved by FDA, shows strong optical absorbance in the NIR region (650–900 nm) due to the charge transition between iron ions Fe^{2+} and Fe^{3+}.

Recently, it has attracted interest for application in PA imaging and PTT [272–275]. Cai et al. [276] utilized hollow mesoporous Prussian blue NPs to develop a theranostic nanoplatform for ultrasound and PA dual-modal imaging-guided chemo-thermal cancer therapy. Anticancer drug, DOX, was loaded into the nanoparticles with relatively high loading capacity due to the mesoporous outer shell and big cavity. Since the drug loaded nanoparticles exhibited excellent photothermal conversion efficiency and high loading capacity, the Prussian blue-based nanoplatform opened a new avenue for chemo-thermal tumor therapy. Chen et al. [277] developed a dual-modal therapy platform fabricated by red blood cell membrane coated hollow mesoporous Prussian blue NPs for the combination of photothermal and chemotherapy. DOX was loaded into the NPs with a loading capacity up to 130%, resulting from the hollow mesoporous structure. Due to the photothermal effect,

Author Manuscript Author Manuscript Author Manuscript Author Manuscript

the DOX release from the NPs was promoted by a NIR laser irradiation. In addition, the acidic tumor microenvironments could also accelerate the DOX release from the NPs.

Apart from metallic nanoparticles, transition metal-based nanomaterials have been reported as theranostic nanoagents for PA imaging-guided therapy as well. Bao et al. [278] synthesized hollow structure PEG-MoO_{3-x} nanospheres for PA imaging-guided chemo-photothermal cancer therapy. The hollow nanospheres had strong LSPR absorption in the NIR region, good biocompatibility, as well as high photothermal conversion efficiency. In addition, due to their large surface area and porous structure, anticancer drug could be loaded into them. Song et al. [279] synthesized polyacrylic acid functionalized Co_9Se_8 nanoplates for PA imaging and MRI-guided chemo-photothermal combinational cancer therapy. The nanoplates demonstrated strong NIR absorption spectrum, T_2 shortening effect, and good photothermal conversion efficiency. Moreover, due to the large surface area to mass ratio, the nanoplates could also act as drug nanocarriers for pH-responsive chemotherapy.

(2) Carbon-based nanomaterials.: CNTs are also explored as drug delivery vehicles for cancer diagnostics and chemotherapies due to their unique properties. For example, Liu et al. [156] developed mesoporous silica (MS) coated SWNTs with polyethylene glycol (PEG) coating for imaging-guided cancer therapy. SWNTs provided strong contrast in both PA imaging and MRI. The PEG coating could improve the stability and solubility of the nanoparticles in a physiological environment. Anticancer drug, DOX, was loaded into the mesoporous structure of the synthesized SWNT@MS-PEG nanoparticle for chemotherapy. Using a low power of laser stimulation and a low dose of DOX, combined photothermal and chemotherapy of cancer tissues was achieved due to the accelerated nanoparticles penetration into cells and the light-triggered drug release.

rGO has an extremely high surface area and strong NIR absorption, and has very high potential to be utilized as a drug or gene delivery vehicle and as a photothermal agent for cancer therapy [280]. For example, Song et al. [166] conjugated DOX with rGO first and then encapsulated of rGO-DOX conjugation in a gold nanorod vesicle (rGO-AuNRVe-DOX) for dual chemo-photothermal therapy. With a relatively low power density of laser irradiation (0.25 W/cm^2), the hybrid vesicle was disrupted and rGO-DOX and DOX was released from the vesicle due to the mild temperature rise in the tumor region with the vesicle injected. Moreover, the increased temperature also resulted in the improved intracellular uptake of DOX for chemotherapy.

3.3.3. Laser-generated ultrasound-accelerated thrombolysis—

Due to its ability to generate high pressure and high frequency shock waves with tight focal spot, laser-generated ultrasound has recently been reported to be utilized for thrombolysis. Compared with existing thrombolysis techniques, the other advantages of laser-generated ultrasound includes its biocompatibility, low cost as well as high clot lysis rate. Kim et al. [281] firstly reported a laser-generated focused ultrasound (LGFU) transducer fabricated by a plano-concave glass lens coated with carbon black/PDMS thermoelastic layer. The transducer could generate shock waves with a central frequency of 14 MHz and peak negative pressure of ~ 12 MPa under a laser energy input of 20 mJ. Combined with 10^8/mL microbubble

Author Manuscript Author Manuscript Author Manuscript Author Manuscript

injection (100 μL/min for 30 min), 29% reduction of blood clot mass was achieved using the LGFU transducer for treatment. Following that, Wu et al. [282] developed a laser-generated ultrasound transducer consisting of candle soot nanoparticles-PDMS composite on an optical fiber for intravascular thrombolysis. It was showed that the fiber-optic laser ultrasound transducer had a central frequency of 6.8 MHz and peak negative pressure of 1.6 MPa under a laser fluence of 1.5 mJ/cm^2. Under the microbubble-mediated thrombolysis test, 32% reduction of blood clot mass was achieved. Most recently, Wu et al. [283] fabricated another fiber-optic laser ultrasound transducer, having the same structure as reported in [282]. The transducer had a central frequency and peak negative pressure of 5.8 MHz and 3.7 MPa, respectively. At the same time of thrombolysis using the developed laser ultrasound transducer, the blood clot status was monitored using a 1064 nm laser source and a commercial linear array transducer based on PA imaging.

4. Conclusions and outlook

In this review, for the first time, the recent progress of nanoacoustics in biomedical imaging and therapy fields was comprehensively examined. The recent advancement made in exploring nanomaterials and nanostructures for biomedical ultrasound and photoacoustic imaging as well as ultrasound and photoacoustic therapies was reviewed in terms of nanomaterials, nanostructures and nanodevice implementations. Based on the literature survey, while many progresses have been made for translating basic scientific research outcomes into routine clinical applications, several obstacles hamper the advancement. Some recommendations for the development of nanoacoustics in biomedical imaging and therapy are outlined here.

Over the past decade, there’s an increasing demand for miniaturized acoustic devices with the growing market shares of mobile devices and internet of things. While conventional piezoelectric acoustic devices currently still dominate the market, there has been extensive studies exploring capacitive micromachined ultrasonic transducers (CMUTs) and piezoelectric micromachined ultrasonic transducers (PMUTs) for various applications, especially for biomedical imaging and therapy. Compared with conventional piezoelectric transducers, one of the key benefits of CMUTs and PMUTs is their easy integration with integrated circuits. Other advantages include their batch production with submicron accuracy and uniformity, low power consumption and compact size.

Many reports focusing on nanosized contrast agents for ultrasound as well as photoacoustic imaging have appeared during the past few years, but the investigations about contrast agents are still largely confined to the research laboratory. While many different kinds of nanosized contrast agent illustrate substantial advantages for imaging applications, the nanomaterials adopted usually possess shortcomings that need to be addressed, including relatively poor biocompatibility, requirements for large doses, low targeting efficiency, and difficulties in accurately quantifying agents. Clearly, many issues still exist and there remains a long road ahead for implementing nanosized contrast agents for clinical applications.

Ultrasound and photoacoustic-mediated drug delivery and therapy using various nanoparticles as drug delivery nanocarriers have demonstrated their great potentials for

Author Manuscript Author Manuscript Author Manuscript Author Manuscript

simultaneous biomedical imaging and synergistic chemotherapy and photoacoustic therapy. While the drug delivery systems fabricated by different nanoparticles are believed to be very promising for future therapeutics, especially oncotherapy, there still exist multiple challenges in the clinical translation of these nanoparticles. For example, although metallic NPs have been reported to have remarkable and tunable acoustic and optical properties, their long-term systemic cytotoxicity and biocompatibility have attracted much concerns from many researchers. In addition, in order to further advance ultrasound and photoacoustic-mediated therapeutic delivery strategies, developing a platform that can monitor the acoustic effect and quantify the drugs delivered into the target tissue in a real-time manner is considered to be very necessary and important. This is particularly crucial for tumor treatment since the tissue-related heterogeneity during drug delivery may bring about incomplete treatment and cancer recurrence.

Acknowledgments

The authors would like to acknowledge the financial support from the National Institutes of Health under the grants R01HL141967, R41HL154735, and R21EB027304; Office of Naval Research under the grant N00014-18-1-2538; and Department of Energy under the grant DE-NE0008708.

References

[1]. Cuenca AG, Jiang H, Hochwald SN, Delano M, Cance WG, Grobmyer SR, Emerging implications of nanotechnology on cancer diagnostics and therapeutics, Cancer. 107 (2006) 459–466. [PubMed: 16795065]

[2]. Farokhzad OC, Langer R, Nanomedicine: developing smarter therapeutic and diagnostic modalities, Adv. Drug Deliv. Rev 58 (2006) 1456–1459. [PubMed: 17070960]

[3]. Nie S, Xing Y, Kim GJ, Simons JW, Nanotechnology applications in cancer, Annu. Rev. Biomed. Eng 9 (2007) 257–288. [PubMed: 17439359]

[4]. Wang X, Yang L, Chen Z, Shin DM, Application of nanotechnology in cancer therapy and imaging, CA. Cancer J. Clin 58 (2008) 97–110. [PubMed: 18227410]

[5]. Barreto JA, O'Malley W, Kubeil M, Graham B, Stephan H, Spiccia L, Nanomaterials: applications in cancer imaging and therapy, Adv. Mater 23 (2011) H18–H40. [PubMed: 21433100]

[6]. Shung KK, Diagnostic ultrasound: Past, present, and future, J Med Biol Eng. 31 (2011) 371–374.

[7]. Kiessling F, Fokong S, Bzyl J, Lederle W, Palmowski M, Lammers T, Recent advances in molecular, multimodal and theranostic ultrasound imaging, Adv. Drug Deliv. Rev 72 (2014) 15–27. doi:10.1016/j.addr.2013.11.013. [PubMed: 24316070]

[8]. Cai Q, Peng C, Prieto JC, Rosenbaum AJ, Stringer JSA, Jiang X, A Low-Cost Camera-Based Ultrasound Probe Tracking System: Design and Prototype, in: 2019 IEEE Int. Ultrason. Symp, IEEE, 2019: pp. 997–999.

[9]. Cai Q, Lu J, Peng C, Prieto JC, Rosenbaum AJ, Stringer JSA, Jiang X, Spatial Calibration for 3D Freehand Ultrasound via Independent General Motions, in: 2020 IEEE Int. Ultrason. Symp, IEEE, 2020: pp. 1–3.

[10]. Hu J, Kim H, Cai Q, Peng C, Chen M, Prieto JC, Rosenbaum AJ, Stringer JSA, Jiang X, Fusion of Ultrasonic Tracking with an Inertial Measurement Unit for High-Accuracy 3D Space Localization, in: 2020 IEEE Int. Ultrason. Symp, IEEE, 2020: pp. 1–4.

[11]. Cai Q, Peng C, Lu J, Prieto JC, Rosenbaum AJ, Stringer JSA, Jiang X, Performance Enhanced Ultrasound Probe Tracking with a Hemispherical Marker Rigid Body, IEEE Trans. Ultrason. Ferroelectr. Freq. Control (2021).

[12]. Perera RH, Hernandez C, Zhou H, Kota P, Burke A, Exner AA, Ultrasound imaging beyond the vasculature with new generation contrast agents, Wiley Interdiscip. Rev. Nanomedicine Nanobiotechnology 7 (2015) 593–608. doi:10.1002/wnan.1326. [PubMed: 25580914]

Author Manuscript Author Manuscript Author Manuscript Author Manuscript

[13]. Peng C, Chen M, Wang H, Shen J, Jiang X, Broadband Piezoelectric Transducers for Under-Display Ultrasonic Fingerprint Sensing Applications, IEEE Trans. Ind. Electron (2020).

[14]. Peng C, Chen M, Wang H, Shen J, Jiang X, P (VDF TrFE) Thin Film Based Transducer for Under Display Ultrasonic Fingerprint Sensing Applications, IEEE Sens. J (2020).

[15]. Peng C, Chen M, Jiang X, Under-Display Ultrasonic Fingerprint Recognition with Finger Vessel Imaging, IEEE Sens. J (2021).

[16]. Abou-Elkacem L, Bachawal SV, Willmann JK, Ultrasound molecular imaging: Moving toward clinical translation, Eur. J. Radiol 84 (2015) 1685–1693. doi:10.1016/j.ejrad.2015.03.016. [PubMed: 25851932]

[17]. Deshpande N, Needles A, Willmann JK, Molecular ultrasound imaging: current status and future directions, Clin. Radiol 65 (2010) 567–581. doi:10.1016/j.crad.2010.02.013. [PubMed: 20541656]

[18]. Klibanov AL, Ligand-carrying gas-filled microbubbles: ultrasound contrast agents for targeted molecular imaging, Bioconjug. Chem 16 (2005) 9–17. [PubMed: 15656569]

[19]. Ibsen S, Schutt CE, Esener S, Microbubble-mediated ultrasound therapy: a review of its potential in cancer treatment, Drug Des. Devel. Ther 7 (2013) 375.

[20]. de Jong N, Hoff L, Skotland T, Bom N, Absorption and scatter of encapsulated gas filled microspheres: theoretical considerations and some measurements, Ultrasonics. 30 (1992) 95–103. [PubMed: 1557838]

[21]. Wu H, Rognin NG, Krupka TM, Solorio L, Yoshiara H, Guenette G, Sanders C, Kamiyama N, Exner AA, Acoustic characterization and pharmacokinetic analyses of new nanobubble ultrasound contrast agents, Ultrasound Med. Biol 39 (2013) 2137–2146. [PubMed: 23932272]

[22]. Perera RH, Solorio L, Wu H, Gangolli M, Silverman E, Hernandez C, Peiris PM, Broome A-M, Exner AA, Nanobubble ultrasound contrast agents for enhanced delivery of thermal sensitizer to tumors undergoing radiofrequency ablation, Pharm. Res 31 (2014) 1407–1417. [PubMed: 23943542]

[23]. Wang Y, Li X, Zhou Y, Huang P, Xu Y, Preparation of nanobubbles for ultrasound imaging and intracelluar drug delivery, Int. J. Pharm 384 (2010) 148–153. [PubMed: 19781609]

[24]. Oeffinger BE, Wheatley MA, Development and characterization of a nano-scale contrast agent, Ultrasonics. 42 (2004) 343–347. [PubMed: 15047309]

[25]. Güvener N, Appold L, de Lorenzi F, Golombek SK, Rizzo LY, Lammers T, Kiessling F, Recent advances in ultrasound-based diagnosis and therapy with micro-and nanometer-sized formulations, Methods. 130 (2017) 4–13. [PubMed: 28552267]

[26]. Tang H, Zheng Y, Chen Y, Materials chemistry of nanoultrasonic biomedicine, Adv. Mater 29 (2017) 1604105.

[27]. Huynh E, Rajora MA, Zheng G, Multimodal micro, nano, and size conversion ultrasound agents for imaging and therapy, Wiley Interdiscip. Rev. Nanomedicine Nanobiotechnology 8 (2016) 796–813. [PubMed: 27006001]

[28]. Perera RH, Hernandez C, Zhou H, Kota P, Burke A, Exner AA, Ultrasound imaging beyond the vasculature with new generation contrast agents, Wiley Interdiscip. Rev. Nanomedicine Nanobiotechnology 7 (2015) 593–608. [PubMed: 25580914]

[29]. Zlitni A, Gambhir SS, Molecular imaging agents for ultrasound, Curr. Opin. Chem. Biol 45 (2018) 113–120. doi:10.1016/j.cbpa.2018.03.017. [PubMed: 29631121]

[30]. Qian X, Han X, Chen Y, Insights into the unique functionality of inorganic micro/nanoparticles for versatile ultrasound theranostics, Biomaterials. 142 (2017) 13–30. [PubMed: 28719818]

[31]. Yang H, Cai W, Xu L, Lv X, Qiao Y, Li P, Wu H, Yang Y, Zhang L, Duan Y, Nanobubble–Affibody: Novel ultrasound contrast agents for targeted molecular ultrasound imaging of tumor, Biomaterials. 37 (2015) 279–288. [PubMed: 25453958]

[32]. Fan X, Wang L, Guo Y, Tu Z, Li L, Tong H, Xu Y, Li R, Fang K, Ultrasonic nanobubbles carrying anti-PSMA nanobody: construction and application in prostate cancer-targeted imaging, PLoS One. 10 (2015) e0127419. [PubMed: 26111008]

[33]. Jiang Q, Hao S, Xiao X, Yao J, Ou B, Zhao Z, Liu F, Pan X, Luo B, Zhi H, Production and characterization of a novel long-acting Herceptin-targeted nanobubble contrast agent specific for Her-2-positive breast cancers, Breast Cancer. 23 (2016) 445–455. [PubMed: 25691133]

Author Manuscript Author Manuscript Author Manuscript Author Manuscript

[34]. Gao Y, Hernandez C, Yuan H-X, Lilly J, Kota P, Zhou H, Wu H, Exner AA, Ultrasound molecular imaging of ovarian cancer with CA-125 targeted nanobubble contrast agents, Nanomedicine Nanotechnology, Biol. Med 13 (2017) 2159–2168.

[35]. Perera RH, Wu H, Peiris P, Hernandez C, Burke A, Zhang H, Exner AA, Improving performance of nanoscale ultrasound contrast agents using N, N-diethylacrylamide stabilization, Nanomedicine Nanotechnology, Biol. Med 13 (2017) 59–67.

[36]. Li K, Liu Y, Zhang S, Xu Y, Jiang J, Yin F, Hu Y, Han B, Ge S, Zhang L, Folate receptor-targeted ultrasonic PFOB nanoparticles: Synthesis, characterization and application in tumor-targeted imaging, Int. J. Mol. Med 39 (2017) 1505–1515. [PubMed: 28487935]

[37]. Liu J, Shang T, Wang F, Cao Y, Hao L, Ren J, Ran H, Wang Z, Li P, Du Z, Low-intensity focused ultrasound (LIFU)-induced acoustic droplet vaporization in phase-transition perfluoropentane nanodroplets modified by folate for ultrasound molecular imaging, Int. J. Nanomedicine 12 (2017) 911. [PubMed: 28184161]

[38]. Choi D, Jeon S, You DG, Um W, Kim J-Y, Yoon HY, Chang H, Kim D-E, Park JH, Kim H, Iodinated echogenic glycol chitosan nanoparticles for X-ray CT/US dual imaging of tumor, Nanotheranostics. 2 (2018) 117. [PubMed: 29577016]

[39]. Xu Y, Niu C, An S, Tang S, Xiao P, Peng Q, Wang L, Thermal-sensitive magnetic nanoparticles for dual-modal tumor imaging and therapy, RSC Adv. 7 (2017) 40791–40802.

[40]. Hannah AS, Luke GP, Emelianov SY, Blinking phase-change nanocapsules enable background-free ultrasound imaging, Theranostics. 6 (2016) 1866. [PubMed: 27570556]

[41]. Yang L, Cheng J, Chen Y, Yu S, Liu F, Sun Y, Chen Y, Ran H, Phase-transition nanodroplets for real-time photoacoustic/ultrasound dual-modality imaging and photothermal therapy of sentinel lymph node in breast cancer, Sci. Rep 7 (2017) 45213. [PubMed: 28338071]

[42]. Cheng Y, Cheng H, Jiang C, Qiu X, Wang K, Huan W, Yuan A, Wu J, Hu Y, Perfluorocarbon nanoparticles enhance reactive oxygen levels and tumour growth inhibition in photodynamic therapy, Nat. Commun 6 (2015) 1–8.

[43]. Zhou Y, Wang R, Teng Z, Wang Z, Hu B, Kolios M, Chen H, Zhang N, Wang Y, Li P, Magnetic nanoparticle-promoted droplet vaporization for in vivo stimuli-responsive cancer theranostics, NPG Asia Mater. 8 (2016) e313–e313.

[44]. Zhang K, Li P, Chen H, Bo X, Li X, Xu H, Continuous cavitation designed for enhancing radiofrequency ablation via a special radiofrequency solidoid vaporization process, ACS Nano. 10 (2016) 2549–2558. [PubMed: 26800221]

[45]. Xu J, Chen Y, Deng L, Liu J, Cao Y, Li P, Ran H, Zheng Y, Wang Z, Microwave-activated nanodroplet vaporization for highly efficient tumor ablation with real-time monitoring performance, Biomaterials. 106 (2016) 264–275. [PubMed: 27573134]

[46]. Min HS, Son S, You DG, Lee TW, Lee J, Lee S, Yhee JY, Lee J, Han MH, Park JH, Chemical gas-generating nanoparticles for tumor-targeted ultrasound imaging and ultrasound-triggered drug delivery, Biomaterials. 108 (2016) 57–70. [PubMed: 27619240]

[47]. Kang C, Cho W, Park M, Kim J, Park S, Shin D, Song C, Lee D, H2O2-triggered bubble generating antioxidant polymeric nanoparticles as ischemia/reperfusion targeted nanotheranostics, Biomaterials. 85 (2016) 195–203. [PubMed: 26874282]

[48]. Zhang N, Li J, Hou R, Zhang J, Wang P, Liu X, Zhang Z, Bubble-generating nano-lipid carriers for ultrasound/CT imaging-guided efficient tumor therapy, Int. J. Pharm 534 (2017) 251–262. [PubMed: 28803939]

[49]. Kim M, Lee JH, Kim SE, Kang SS, Tae G, Nanosized ultrasound enhanced-contrast agent for in vivo tumor imaging via intravenous injection, ACS Appl. Mater. Interfaces 8 (2016) 8409–8418. [PubMed: 27010717]

[50]. Feng Q, Zhang W, Yang X, Li Y, Hao Y, Zhang H, Hou L, Zhang Z, pH/Ultrasound Dual-Responsive Gas Generator for Ultrasound Imaging-Guided Therapeutic Inertial Cavitation and Sonodynamic Therapy, Adv. Healthc. Mater 7 (2018) 1700957.

[51]. Lee J, Min H-S, You DG, Kim K, Kwon IC, Rhim T, Lee KY, Theranostic gas-generating nanoparticles for targeted ultrasound imaging and treatment of neuroblastoma, J. Control. Release 223 (2016) 197–206. [PubMed: 26739549]

Author Manuscript Author Manuscript Author Manuscript Author Manuscript

[52]. Min KH, Min HS, Lee HJ, Park DJ, Yhee JY, Kim K, Kwon IC, Jeong SY, Silvestre OF, Chen X, pH-controlled gas-generating mineralized nanoparticles: a theranostic agent for ultrasound imaging and therapy of cancers, ACS Nano. 9 (2015) 134–145. [PubMed: 25559896]

[53]. Wang X, Niu D, Li P, Wu Q, Bo X, Liu B, Bao S, Su T, Xu H, Wang Q, Dual-enzyme-loaded multifunctional hybrid nanogel system for pathological responsive ultrasound imaging and T 2-weighted magnetic resonance imaging, ACS Nano. 9 (2015) 5646–5656. [PubMed: 26035730]

[54]. Gao S, Wang G, Qin Z, Wang X, Zhao G, Ma Q, Zhu L, Oxygen-generating hybrid nanoparticles to enhance fluorescent/photoacoustic/ultrasound imaging guided tumor photodynamic therapy, Biomaterials. 112 (2017) 324–335. [PubMed: 27776285]

[55]. Casciaro S, Conversano F, Ragusa A, Malvindi MA, Franchini R, Greco A, Pellegrino T, Gigli G, Optimal enhancement configuration of silica nanoparticles for ultrasound imaging and automatic detection at conventional diagnostic frequencies, Invest. Radiol 45 (2010) 715–724. [PubMed: 20562708]

[56]. Hu H, Zhou H, Du J, Wang Z, An L, Yang H, Li F, Wu H, Yang S, Biocompatiable hollow silica microspheres as novel ultrasound contrast agents for in vivo imaging, J. Mater. Chem 21 (2011) 6576–6583.

[57]. Martinez HP, Kono Y, Blair SL, Sandoval S, Wang-Rodriguez J, Mattrey RF, Kummel AC, Trogler WC, Hard shell gas-filled contrast enhancement particles for colour Doppler ultrasound imaging of tumors, Medchemcomm. 1 (2010) 266–270. [PubMed: 21841967]

[58]. Milgroom A, Intrator M, Madhavan K, Mazzaro L, Shandas R, Liu B, Park D, Mesoporous silica nanoparticles as a breast-cancer targeting ultrasound contrast agent, Colloids Surfaces B Biointerfaces. 116 (2014) 652–657. [PubMed: 24269054]

[59]. Jin Q, Lin C-Y, Kang S-T, Chang Y-C, Zheng H, Yang C-M, Yeh C-K, Superhydrophobic silica nanoparticles as ultrasound contrast agents, Ultrason. Sonochem 36 (2017) 262–269. [PubMed: 28069209]

[60]. Zhang K, Chen H, Guo X, Zhang D, Zheng Y, Zheng H, Shi J, Doublescattering/reflection in a single nanoparticle for intensified ultrasound imaging, Sci. Rep 5 (2015) 1–11.

[61]. Chen F, Ma M, Wang J, Wang F, Chern S-X, Zhao ER, Jhunjhunwala A, Darmadi S, Chen H, V Jokerst J, Exosome-like silica nanoparticles: a novel ultrasound contrast agent for stem cell imaging, Nanoscale. 9 (2017) 402–411. [PubMed: 27924340]

[62]. Liberman A, Wang J, Lu N, Viveros RD, Allen CA, Mattrey RF, Blair SL, Trogler WC, Kim MJ, Kummel AC, Mechanically tunable hollow silica ultrathin nanoshells for ultrasound contrast agents, Adv. Funct. Mater 25 (2015) 4049–4057. [PubMed: 26955300]

[63]. Sun Y, Wang Y, Niu C, Strohm EM, Zheng Y, Ran H, Huang R, Zhou D, Gong Y, Wang Z, Laser-activatible PLGA microparticles for image-guided cancer therapy in vivo, Adv. Funct. Mater 24 (2014) 7674–7680.

[64]. Ke H, Wang J, Tong S, Jin Y, Wang S, Qu E, Bao G, Dai Z, Gold nanoshelled liquid perfluorocarbon magnetic nanocapsules: a nanotheranostic platform for bimodal ultrasound/ magnetic resonance imaging guided photothermal tumor ablation, Theranostics. 4 (2014) 12.

[65]. Prasad P, Gordijo CR, Abbasi AZ, Maeda A, Ip A, Rauth AM, DaCosta RS, Wu XY, Multifunctional albumin–MnO2 nanoparticles modulate solid tumor microenvironment by attenuating hypoxia, acidosis, vascular endothelial growth factor and enhance radiation response, ACS Nano. 8 (2014) 3202–3212. [PubMed: 24702320]

[66]. Yang F, Hu S, Zhang Y, Cai X, Huang Y, Wang F, Wen S, Teng G, Gu N, A Hydrogen Peroxide-Responsive O2 Nanogenerator for Ultrasound and Magnetic-Resonance Dual Modality Imaging, Adv. Mater 24 (2012) 5205–5211. [PubMed: 22811026]

[67]. Jia X, Cai X, Chen Y, Wang S, Xu H, Zhang K, Ma M, Wu H, Shi J, Chen H, Perfluoropentane-encapsulated hollow mesoporous prussian blue nanocubes for activated ultrasound imaging and photothermal therapy of cancer, ACS Appl. Mater. Interfaces 7 (2015) 4579–4588. [PubMed: 25646576]

[68]. Delogu LG, Vidili G, Venturelli E, Ménard-Moyon C, Zoroddu MA, Pilo G, Nicolussi P, Ligios C, Bedognetti D, Sgarrella F, Functionalized multiwalled carbon nanotubes as ultrasound contrast agents, Proc. Natl. Acad. Sci 109 (2012) 16612–16617. [PubMed: 23012426]

Author Manuscript Author Manuscript Author Manuscript Author Manuscript

[69]. Wu H, Shi H, Zhang H, Wang X, Yang Y, Yu C, Hao C, Du J, Hu H, Yang S, Prostate stem cell antigen antibody-conjugated multiwalled carbon nanotubes for targeted ultrasound imaging and drug delivery, Biomaterials. 35 (2014) 5369–5380. [PubMed: 24709520]

[70]. Walsby AE, Gas vesicles, Microbiol. Mol. Biol. Rev 58 (1994) 94–144.

[71]. Pfeifer F, Distribution, formation and regulation of gas vesicles, Nat. Rev. Microbiol 10 (2012) 705. [PubMed: 22941504]

[72]. Shapiro MG, Goodwill PW, Neogy A, Yin M, Foster FS, V Schaffer D, Conolly SM, Biogenic gas nanostructures as ultrasonic molecular reporters, Nat. Nanotechnol 9 (2014) 311. [PubMed: 24633522]

[73]. Cherin E, Melis JM, Bourdeau RW, Yin M, Kochmann DM, Foster FS, Shapiro MG, Acoustic behavior of Halobacterium salinarum gas vesicles in the high-frequency range: experiments and modeling, Ultrasound Med. Biol 43 (2017) 1016–1030. [PubMed: 28258771]

[74]. Zhang S, Huang A, Bar-Zion A, Wang J, Mena OV, Shapiro MG, Friend J, The Vibration Behavior of Sub-Micrometer Gas Vesicles in Response to Acoustic Excitation Determined via Laser Doppler Vibrometry, Adv. Funct. Mater 30 (2020) 2000239.

[75]. Lakshmanan A, Farhadi A, Nety SP, Lee-Gosselin A, Bourdeau RW, Maresca D, Shapiro MG, Molecular engineering of acoustic protein nanostructures, ACS Nano. 10 (2016) 7314–7322. [PubMed: 27351374]

[76]. Lakshmanan A, Lu GJ, Farhadi A, Nety SP, Kunth M, Lee-Gosselin A, Maresca D, Bourdeau RW, Yin M, Yan J, Preparation of biogenic gas vesicle nanostructures for use as contrast agents for ultrasound and MRI, Nat. Protoc 12 (2017) 2050. [PubMed: 28880278]

[77]. Le Floc'h J, Zlitni A, Bilton HA, Yin M, Farhadi A, Janzen NR, Shapiro MG, Valliant JF, Foster FS, In vivo Biodistribution of Radiolabeled Acoustic Protein Nanostructures, Mol. Imaging Biol 20 (2018) 230–239. [PubMed: 28956265]

[78]. Maresca D, Lakshmanan A, Lee-Gosselin A, Melis JM, Ni Y-L, Bourdeau RW, Kochmann DM, Shapiro MG, Nonlinear ultrasound imaging of nanoscale acoustic biomolecules, Appl. Phys. Lett 110 (2017) 73704.

[79]. Yan J, Yin M, Foster FS, Démoré CEM, Tumor contrast imaging with gas vesicles by circumventing the reticuloendothelial system, Ultrasound Med. Biol 46 (2020) 359–368. [PubMed: 31708270]

[80]. Lu GJ, Chou L, Malounda D, Patel AK, Welsbie DS, Chao DL, Ramalingam T, Shapiro MG, Genetically encodable contrast agents for optical coherence tomography, ACS Nano. (2020).

[81]. Bourdeau RW, Lee-Gosselin A, Lakshmanan A, Farhadi A, Kumar SR, Nety SP, Shapiro MG, Acoustic reporter genes for noninvasive imaging of microorganisms in mammalian hosts, Nature. 553 (2018) 86. [PubMed: 29300010]

[82]. Farhadi A, Ho GH, Sawyer DP, Bourdeau RW, Shapiro MG, Ultrasound imaging of gene expression in mammalian cells, Science (80-.) 365 (2019) 1469–1475.

[83]. Lu GJ, Farhadi A, Mukherjee A, Shapiro MG, Proteins, air and water: reporter genes for ultrasound and magnetic resonance imaging, Curr. Opin. Chem. Biol 45 (2018) 57–63. doi:10.1016/j.cbpa.2018.02.011. [PubMed: 29549770]

[84]. Wu D, Huang L, Jiang MS, Jiang H, Contrast agents for photoacoustic and thermoacoustic imaging: a review, Int. J. Mol. Sci 15 (2014) 23616–23639. [PubMed: 25530615]

[85]. Wang S, Lin J, Wang T, Chen X, Huang P, Recent advances in photoacoustic imaging for deep-tissue biomedical applications, Theranostics. 6 (2016) 2394. [PubMed: 27877243]

[86]. Gargiulo S, Albanese S, Mancini M, State-of-the-Art preclinical photoacoustic imaging in oncology: recent advances in cancer theranostics, Contrast Media Mol. Imaging 2019 (2019).

[87]. Yoo SW, Jung D, Min J-J, Kim H, Lee C, Biodegradable contrast agents for photoacoustic imaging, Appl. Sci 8 (2018) 1567.

[88]. Zhang Y, Jeon M, Rich LJ, Hong H, Geng J, Zhang Y, Shi S, Barnhart TE, Alexandridis P, Huizinga JD, Non-invasive multimodal functional imaging of the intestine with frozen micellar naphthalocyanines, Nat. Nanotechnol 9 (2014) 631. [PubMed: 24997526]

[89]. Lee D, Lee C, Kim S, Zhou Q, Kim J, Kim C, In vivo near infrared virtual intraoperative surgical photoacoustic optical coherence tomography, Sci. Rep 6 (2016) 35176. [PubMed: 27731390]

Author Manuscript Author Manuscript Author Manuscript Author Manuscript

[90]. Park K, Kim JY, Lee C, Jeon S, Lim G, Kim C, Handheld photoacoustic microscopy probe, Sci. Rep 7 (2017) 1–15. [PubMed: 28127051]

[91]. Hu S, V Wang L, Neurovascular photoacoustic tomography, Front. Neuroenergetics 2 (2010) 10. [PubMed: 20616885]

[92]. Yao J, Maslov KI, Zhang Y, Xia Y, V Wang L, Label-free oxygen-metabolic photoacoustic microscopy in vivo, J. Biomed. Opt 16 (2011) 76003.

[93]. Zhang C, V Wang L, Cheng Y-J, Chen J, Wickline SA, Label-free photoacoustic microscopy of myocardial sheet architecture, J. Biomed. Opt 17 (2012) 60506.

[94]. Zhou Y, Xing W, Maslov KI, Cornelius LA, V Wang L, Handheld photoacoustic microscopy to detect melanoma depth in vivo, Opt. Lett 39 (2014) 4731–4734. [PubMed: 25121860]

[95]. V Wang L, Multiscale photoacoustic microscopy and computed tomography, Nat. Photonics 3 (2009) 503. [PubMed: 20161535]

[96]. Xu M, Wang LV, Photoacoustic imaging in biomedicine, Rev. Sci. Instrum 77 (2006) 041101. doi:10.1063/1.2195024.

[97]. Weber J, Beard PC, Bohndiek SE, Contrast agents for molecular photoacoustic imaging, Nat. Methods 13 (2016) 639–650. [PubMed: 27467727]

[98]. Fan Q, Cheng K, Yang Z, Zhang R, Yang M, Hu X, Ma X, Bu L, Lu X, Xiong X, Perylene-diimide-based nanoparticles as highly efficient photoacoustic agents for deep brain tumor imaging in living mice, Adv. Mater 27 (2015) 843–847. [PubMed: 25376906]

[99]. Kircher MF, De La Zerda A, V Jokerst J, Zavaleta CL, Kempen PJ, Mittra E, Pitter K, Huang R, Campos C, Habte F, A brain tumor molecular imaging strategy using a new triple-modality MRI-photoacoustic-Raman nanoparticle, Nat. Med 18 (2012) 829–834. [PubMed: 22504484]

[100]. Liu J, Cai X, Pan H, Bandla A, Chuan CK, Wang S, Thakor N, Liao L, Liu B, Molecular engineering of photoacoustic performance by chalcogenide variation in conjugated polymer nanoparticles for brain vascular imaging, Small. 14 (2018) 1703732.

[101]. Liu C, Chen J, Zhu Y, Gong X, Zheng R, Chen N, Chen D, Yan H, Zhang P, Zheng H, Highly sensitive MoS 2–indocyanine green hybrid for photoacoustic imaging of orthotopic brain glioma at deep site, Nano-Micro Lett. 10 (2018) 48.

[102]. Kang J, Kim D, Wang J, Han Y, Zuidema JM, Hariri A, Park J, V Jokerst J, Sailor MJ, Enhanced performance of a molecular photoacoustic imaging agent by encapsulation in mesoporous silicon nanoparticles, Adv. Mater 30 (2018) 1800512.

[103]. Wu C, Zhang Y, Li Z, Li C, Wang Q, A novel photoacoustic nanoprobe of ICG@ PEG-Ag 2 S for atherosclerosis targeting and imaging in vivo, Nanoscale. 8 (2016) 12531–12539. [PubMed: 26853187]

[104]. Jung E, Kang C, Lee J, Yoo D, Hwang DW, Kim D, Park S-C, Lim SK, Song C, Lee D, Molecularly engineered theranostic nanoparticles for thrombosed vessels: H2O2-activatable contrast-enhanced photoacoustic imaging and antithrombotic therapy, ACS Nano. 12 (2018) 392–401. [PubMed: 29257881]

[105]. Cui C, Yang Z, Hu X, Wu J, Shou K, Ma H, Jian C, Zhao Y, Qi B, Hu X, Organic semiconducting nanoparticles as efficient photoacoustic agents for lightening early thrombus and monitoring thrombolysis in living mice, ACS Nano. 11 (2017) 3298–3310. [PubMed: 28240881]

[106]. Luke GP, Bashyam A, Homan KA, Makhija S, Chen Y-S, Emelianov SY, Silica-coated gold nanoplates as stable photoacoustic contrast agents for sentinel lymph node imaging, Nanotechnology. 24 (2013) 455101. [PubMed: 24121616]

[107]. Pu K, Shuhendler AJ, V Jokerst J, Mei J, Gambhir SS, Bao Z, Rao J, Semiconducting polymer nanoparticles as photoacoustic molecular imaging probes in living mice, Nat. Nanotechnol 9 (2014) 233. [PubMed: 24463363]

[108]. Cai X, Liu X, Liao L, Bandla A, Ling JM, Liu Y, Thakor N, Bazan GC, Liu B, Encapsulated conjugated oligomer nanoparticles for real-time photoacoustic sentinel lymph node imaging and targeted photothermal therapy, Small. 12 (2016) 4873–4880. [PubMed: 27439884]

[109]. Santiesteban DY, Dumani DS, Profili D, Emelianov SY, Copper sulfide perfluorocarbon nanodroplets as clinically relevant photoacoustic/ultrasound imaging agents, Nano Lett. 17 (2017) 5984–5989. [PubMed: 28926263]

Author Manuscript Author Manuscript Author Manuscript Author Manuscript

[110]. Knox HJ, Kim TW, Zhu Z, Chan J, Photophysical tuning of N-oxide-based probes enables ratiometric photoacoustic imaging of tumor hypoxia, ACS Chem. Biol 13 (2018) 1838–1843. [PubMed: 29521492]

[111]. Chen Q, Liu X, Chen J, Zeng J, Cheng Z, Liu Z, A self-assembled albumin-based nanoprobe for in vivo ratiometric photoacoustic pH imaging, Adv. Mater 27 (2015) 6820–6827. [PubMed: 26418312]

[112]. Miao Q, Lyu Y, Ding D, Pu K, Semiconducting oligomer nanoparticles as an activatable photoacoustic probe with amplified brightness for in vivo imaging of pH, Adv. Mater 28 (2016) 3662–3668. [PubMed: 27000431]

[113]. Cash KJ, Li C, Xia J, V Wang L, Clark HA, Optical drug monitoring: photoacoustic imaging of nanosensors to monitor therapeutic lithium in vivo, ACS Nano. 9 (2015) 1692–1698. [PubMed: 25588028]

[114]. Liu Y, Wang S, Ma Y, Lin J, Wang H, Gu Y, Chen X, Huang P, Ratiometric photoacoustic molecular imaging for methylmercury detection in living subjects, Adv. Mater 29 (2017) 1606129.

[115]. Fu Q, Zhu R, Song J, Yang H, Chen X, Photoacoustic imaging: contrast agents and their biomedical applications, Adv. Mater 31 (2019) 1805875.

[116]. Tang W, Yang Z, Wang S, Wang Z, Song J, Yu G, Fan W, Dai Y, Wang J, Shan L, Organic semiconducting photoacoustic nanodroplets for laser-activatable ultrasound imaging and combinational cancer therapy, ACS Nano. 12 (2018) 2610–2622. [PubMed: 29451774]

[117]. Petryayeva E, Krull UJ, Localized surface plasmon resonance: Nanostructures, bioassays and biosensing—A review, Anal. Chim. Acta 706 (2011) 8–24. [PubMed: 21995909]

[118]. Cao J, Sun T, V Grattan KT, Gold nanorod-based localized surface plasmon resonance biosensors: A review, Sensors Actuators B Chem. 195 (2014) 332–351.

[119]. Lu W, Melancon MP, Xiong C, Huang Q, Elliott A, Song S, Zhang R, Flores LG, Gelovani JG, V Wang L, Effects of photoacoustic imaging and photothermal ablation therapy mediated by targeted hollow gold nanospheres in an orthotopic mouse xenograft model of glioma, Cancer Res. 71 (2011) 6116–6121. [PubMed: 21856744]

[120]. Wei C, Lombardo M, Larson-Smith K, Pelivanov I, Perez C, Xia J, Matula T, Pozzo D, O'Donnell M, Nonlinear contrast enhancement in photoacoustic molecular imaging with gold nanosphere encapsulated nanoemulsions, Appl. Phys. Lett 104 (2014) 33701.

[121]. Prost A, Poisson F, Bossy E, Photoacoustic generation by a gold nanosphere: From linear to nonlinear thermoelastics in the long-pulse illumination regime, Phys. Rev. B 92 (2015) 115450.

[122]. Chen P-J, Hu S-H, Fan C-T, Li M-L, Chen Y-Y, Chen S-Y, Liu D-M, A novel multifunctional nano-platform with enhanced anti-cancer and photoacoustic imaging modalities using gold-nanorod-filled silica nanobeads, Chem. Commun 49 (2013) 892–894.

[123]. Song J, Yang X, Jacobson O, Huang P, Sun X, Lin L, Yan X, Niu G, Ma Q, Chen X, Ultrasmall gold nanorod vesicles with enhanced tumor accumulation and fast excretion from the body for cancer therapy, Adv. Mater 27 (2015) 4910–4917. [PubMed: 26198622]

[124]. Zhong J, Wen L, Yang S, Xiang L, Chen Q, Xing D, Imaging-guided high-efficient photoacoustic tumor therapy with targeting gold nanorods, Nanomedicine Nanotechnology, Biol. Med 11 (2015) 1499–1509.

[125]. Yan N, Wang X, Lin L, Song T, Sun P, Tian H, Liang H, Chen X, Gold Nanorods Electrostatically Binding Nucleic Acid Probe for In Vivo MicroRNA Amplified Detection and Photoacoustic Imaging-Guided Photothermal Therapy, Adv. Funct. Mater 28 (2018) 1800490.

[126]. Pérez-Hernández M, del Pino P, Mitchell SG, Moros M, Stepien G, Pelaz B, Parak WJ, Gálvez EM, Pardo J, de la Fuente JM, Dissecting the molecular mechanism of apoptosis during photothermal therapy using gold nanoprisms, ACS Nano. 9 (2015) 52–61. [PubMed: 25493329]

[127]. Bao C, Conde J, Pan F, Li C, Zhang C, Tian F, Liang S, Jesus M, Cui D, Gold nanoprisms as a hybrid in vivo cancer theranostic platform for in situ photoacoustic imaging, angiography, and localized hyperthermia, Nano Res. 9 (2016) 1043–1056.

[128]. Bao C, Beziere N, del Pino P, Pelaz B, Estrada G, Tian F, Ntziachristos V, de la Fuente JM, Cui D, Gold nanoprisms as optoacoustic signal nanoamplifiers for in vivo bioimaging of gastrointestinal cancers, Small. 9 (2013) 68–74. [PubMed: 23001862]

Author Manuscript Author Manuscript Author Manuscript Author Manuscript

[129]. Kim C, Cho EC, Chen J, Song KH, Au L, Favazza C, Zhang Q, Cobley CM, Gao F, Xia Y, In vivo molecular photoacoustic tomography of melanomas targeted by bioconjugated gold nanocages, ACS Nano. 4 (2010) 4559–4564. [PubMed: 20731439]

[130]. Moon GD, Choi S-W, Cai X, Li W, Cho EC, Jeong U, V Wang L, Xia Y, A new theranostic system based on gold nanocages and phase-change materials with unique features for photoacoustic imaging and controlled release, J. Am. Chem. Soc 133 (2011) 4762–4765. [PubMed: 21401092]

[131]. Liang R, Xie J, Li J, Wang K, Liu L, Gao Y, Hussain M, Shen G, Zhu J, Tao J, Liposomes-coated gold nanocages with antigens and adjuvants targeted delivery to dendritic cells for enhancing antitumor immune response, Biomaterials. 149 (2017) 41–50. [PubMed: 28992509]

[132]. An J, Yang X-Q, Cheng K, Song X-L, Zhang L, Li C, Zhang X-S, Xuan Y, Song Y-Y, Fang B-Y, In Vivo Computed Tomography/Photoacoustic Imaging and NIR-Triggered Chemo–Photothermal Combined Therapy Based on a Gold Nanostar-, Mesoporous Silica-, and Thermosensitive Liposome-Composited Nanoprobe, ACS Appl. Mater. Interfaces 9 (2017) 41748–41759. [PubMed: 29124936]

[133]. Li X, Xing L, Zheng K, Wei P, Du L, Shen M, Shi X, Formation of gold nanostarcoated hollow mesoporous silica for tumor multimodality imaging and photothermal therapy, ACS Appl. Mater. Interfaces 9 (2017) 5817–5827. [PubMed: 28118704]

[134]. Raghavan V, O'Flatharta C, Dwyer R, Breathnach A, Zafar H, Dockery P, Wheatley A, Keogh I, Leahy M, Olivo M, Dual plasmonic gold nanostars for photoacoustic imaging and photothermal therapy, Nanomedicine. 12 (2017) 457–471. [PubMed: 28181456]

[135]. Chen M, Tang S, Guo Z, Wang X, Mo S, Huang X, Liu G, Zheng N, Core–Shell Pd@Au Nanoplates as Theranostic Agents for In-Vivo Photoacoustic Imaging, CT Imaging, and Photothermal Therapy, Adv. Mater 26 (2014) 8210–8216. [PubMed: 25363309]

[136]. Morsin M, Mat Salleh M, Ali Umar A, Sahdan MZ, Gold nanoplates for a localized surface plasmon resonance-based boric acid sensor, Sensors. 17 (2017) 947.

[137]. Yu Q, Guan P, Qin D, Golden G, Wallace PM, Inverted size-dependence of surface-enhanced Raman scattering on gold nanohole and nanodisk arrays, Nano Lett. 8 (2008) 1923–1928. [PubMed: 18563939]

[138]. Zoric I, Zach M, Kasemo B, Langhammer C, Gold, platinum, and aluminum nanodisk plasmons: material independence, subradiance, and damping mechanisms, ACS Nano. 5 (2011) 2535–2546. [PubMed: 21438568]

[139]. Wi J-S, Park J, Kang H, Jung D, Lee S-W, Lee TG, Stacked gold nanodisks for bimodal photoacoustic and optical coherence imaging, ACS Nano. 11 (2017) 6225–6232. [PubMed: 28531347]

[140]. Zhao J, Wallace M, Melancon MP, Cancer theranostics with gold nanoshells, Nanomedicine. 9 (2014) 2041–2057. [PubMed: 25343352]

[141]. Weber V, Feis A, Gellini C, Pilot R, Salvi PR, Signorini R, Far-and near-field properties of gold nanoshells studied by photoacoustic and surface-enhanced Raman spectroscopies, Phys. Chem. Chem. Phys 17 (2015) 21190–21197. [PubMed: 25559555]

[142]. Song J, Yang X, Yang Z, Lin L, Liu Y, Zhou Z, Shen Z, Yu G, Dai Y, Jacobson O, Rational design of branched nanoporous gold nanoshells with enhanced physico-optical properties for optical imaging and cancer therapy, ACS Nano. 11 (2017) 6102–6113. [PubMed: 28605594]

[143]. Cheng K, Kothapalli S-R, Liu H, Koh AL, V Jokerst J, Jiang H, Yang M, Li J, Levi J, Wu JC, Construction and validation of nano gold tripods for molecular imaging of living subjects, J. Am. Chem. Soc 136 (2014) 3560–3571. [PubMed: 24495038]

[144]. Liu Y, Yang Z, Huang X, Yu G, Wang S, Zhou Z, Shen Z, Fan W, Liu Y, Davisson M, Glutathione-responsive self-assembled magnetic gold nanowreath for enhanced tumor imaging and imaging-guided photothermal therapy, ACS Nano. 12 (2018) 8129–8137. [PubMed: 30001110]

[145]. Huang P, Pandoli O, Wang X, Wang Z, Li Z, Zhang C, Chen F, Lin J, Cui D, Chen X, Chiral guanosine 5′-monophosphate-capped gold nanoflowers: Controllable synthesis, characterization, surface-enhanced Raman scattering activity, cellular imaging and photothermal therapy, Nano Res. 5 (2012) 630–639.

Author Manuscript Author Manuscript Author Manuscript Author Manuscript

[146]. Huang P, Rong P, Lin J, Li W, Yan X, Zhang MG, Nie L, Niu G, Lu J, Wang W, Triphase interface synthesis of plasmonic gold bellflowers as near-infrared light mediated acoustic and thermal theranostics, J. Am. Chem. Soc 136 (2014) 8307–8313. [PubMed: 24842342]

[147]. Personick ML, Langille MR, Zhang J, Harris N, Schatz GC, Mirkin CA, Synthesis and isolation of {110}-faceted gold bipyramids and rhombic dodecahedra, J. Am. Chem. Soc 133 (2011) 6170–6173. [PubMed: 21452816]

[148]. Lu W, Huang Q, Ku G, Wen X, Zhou M, Guzatov D, Brecht P, Su R, Oraevsky A, V Wang L, Photoacoustic imaging of living mouse brain vasculature using hollow gold nanospheres, Biomaterials. 31 (2010) 2617–2626. [PubMed: 20036000]

[149]. V Jokerst J, Cole AJ, Van de Sompel D, Gambhir SS, Gold nanorods for ovarian cancer detection with photoacoustic imaging and resection guidance via Raman imaging in living mice, ACS Nano. 6 (2012) 10366–10377. [PubMed: 23101432]

[150]. Wang W, Hao C, Sun M, Xu L, Xu C, Kuang H, Spiky Fe3O4@ Au supraparticles for multimodal in vivo imaging, Adv. Funct. Mater 28 (2018) 1800310.

[151]. Bai L-Y, Yang X-Q, An J, Zhang L, Zhao K, Qin M-Y, Fang B-Y, Li C, Xuan Y, Zhang X-S, Multifunctional magnetic-hollow gold nanospheres for bimodal cancer cell imaging and photothermal therapy, Nanotechnology. 26 (2015) 315701. [PubMed: 26177713]

[152]. Song J, Cheng L, Liu A, Yin J, Kuang M, Duan H, Plasmonic vesicles of amphiphilic gold nanocrystals: self-assembly and external-stimuli-triggered destruction, J. Am. Chem. Soc 133 (2011) 10760–10763. [PubMed: 21699155]

[153]. Deng H, Dai F, Ma G, Zhang X, Theranostic gold nanomicelles made from biocompatible comb-like polymers for thermochemotherapy and multifunctional imaging with rapid clearance, Adv. Mater 27 (2015) 3645–3653. [PubMed: 25946668]

[154]. Meng L, Zhang X, Lu Q, Fei Z, Dyson PJ, Single walled carbon nanotubes as drug delivery vehicles: targeting doxorubicin to tumors, Biomaterials. 33 (2012) 1689–1698. [PubMed: 22137127]

[155]. Gong H, Peng R, Liu Z, Carbon nanotubes for biomedical imaging: the recent advances, Adv. Drug Deliv. Rev 65 (2013) 1951–1963. [PubMed: 24184130]

[156]. Liu J, Wang C, Wang X, Wang X, Cheng L, Li Y, Liu Z, Mesoporous silica coated single-walled carbon nanotubes as a multifunctional light-responsive platform for cancer combination therapy, Adv. Funct. Mater 25 (2015) 384–392.

[157]. Lalwani G, Cai X, Nie L, V Wang L, Sitharaman B, Graphene-based contrast agents for photoacoustic and thermoacoustic tomography, Photoacoustics. 1 (2013) 62–67. [PubMed: 24490141]

[158]. Chen Y, Tan C, Zhang H, Wang L, Two-dimensional graphene analogues for biomedical applications, Chem. Soc. Rev 44 (2015) 2681–2701. [PubMed: 25519856]

[159]. Hu D, Zhang J, Gao G, Sheng Z, Cui H, Cai L, Indocyanine green-loaded polydopamine-reduced graphene oxide nanocomposites with amplifying photoacoustic and photothermal effects for cancer theranostics, Theranostics. 6 (2016) 1043. [PubMed: 27217837]

[160]. Toumia Y, Domenici F, Orlanducci S, Mura F, Grishenkov D, Trochet P, Lacerenza S, Bordi F, Paradossi G, Graphene meets microbubbles: A superior contrast agent for photoacoustic imaging, ACS Appl. Mater. Interfaces 8 (2016) 16465–16475. [PubMed: 27269868]

[161]. Yang F, Song W, Zhang C, Min C, Fang H, Du L, Wu P, Zheng W, Li C, Zhu S, Broadband graphene-based photoacoustic microscopy with high sensitivity, Nanoscale. 10 (2018) 8606–8614. [PubMed: 29696248]

[162]. De La Zerda A, Zavaleta C, Keren S, Vaithilingam S, Bodapati S, Liu Z, Levi J, Smith BR, Ma T-J, Oralkan O, Carbon nanotubes as photoacoustic molecular imaging agents in living mice, Nat. Nanotechnol 3 (2008) 557. [PubMed: 18772918]

[163]. Kim J-W, Galanzha EI, V Shashkov E, Moon H-M, Zharov VP, Golden carbon nanotubes as multimodal photoacoustic and photothermal high-contrast molecular agents, Nat. Nanotechnol 4 (2009) 688. [PubMed: 19809462]

[164]. Song J, Wang F, Yang X, Ning B, Harp MG, Culp SH, Hu S, Huang P, Nie L, Chen J, Gold nanoparticle coated carbon nanotube ring with enhanced raman scattering and photothermal

Author Manuscript Author Manuscript Author Manuscript Author Manuscript

conversion property for theranostic applications, J. Am. Chem. Soc 138 (2016) 7005–7015. [PubMed: 27193381]

[165]. Moon H, Kumar D, Kim H, Sim C, Chang J-H, Kim J-M, Kim H, Lim D-K, Amplified photoacoustic performance and enhanced photothermal stability of reduced graphene oxide coated gold nanorods for sensitive photoacoustic imaging, ACS Nano. 9 (2015) 2711–2719. [PubMed: 25751167]

[166]. Song J, Yang X, Jacobson O, Lin L, Huang P, Niu G, Ma Q, Chen X, Sequential drug release and enhanced photothermal and photoacoustic effect of hybrid reduced graphene oxide-loaded ultrasmall gold nanorod vesicles for cancer therapy, ACS Nano. 9 (2015) 9199–9209. [PubMed: 26308265]

[167]. Biswas C, Lee YH, Graphene versus carbon nanotubes in electronic devices, Adv. Funct. Mater 21 (2011) 3806–3826.

[168]. Lentacker I, De Cock I, Deckers R, De Smedt SC, Moonen CTW, Understanding ultrasound induced sonoporation: Definitions and underlying mechanisms, Adv. Drug Deliv. Rev 72 (2014) 49–64. doi:10.1016/j.addr.2013.11.008. [PubMed: 24270006]

[169]. Wang T-Y, E Wilson K, Machtaler S, K Willmann J, Ultrasound and microbubble guided drug delivery: mechanistic understanding and clinical implications, Curr. Pharm. Biotechnol 14 (2013) 743–752. [PubMed: 24372231]

[170]. Chowdhury SM, Wang T-Y, Bachawal S, Devulapally R, Choe JW, Elkacem LA, Yakub BK, Wang DS, Tian L, Paulmurugan R, Ultrasound-guided therapeutic modulation of hepatocellular carcinoma using complementary microRNAs, J. Control. Release 238 (2016) 272–280. [PubMed: 27503707]

[171]. Dewitte H, Vanderperren K, Haers H, Stock E, Duchateau L, Hesta M, Saunders JH, De Smedt SC, Lentacker I, Theranostic mRNA-loaded microbubbles in the lymphatics of dogs: implications for drug delivery, Theranostics. 5 (2015) 97. [PubMed: 25553101]

[172]. Xie X, Lin W, Liu H, Deng J, Chen Y, Liu H, Fu X, Yang Y, Ultrasoundresponsive nanobubbles contained with peptide–camptothecin conjugates for targeted drug delivery, Drug Deliv. 23 (2016) 2756–2764. [PubMed: 26289216]

[173]. Schoellhammer CM, Lauwers GY, Goettel JA, Oberli MA, Cleveland C, Park JY, Minahan D, Chen Y, Anderson DG, Jaklenec A, Ultrasound-mediated delivery of RNA to colonic mucosa of live mice, Gastroenterology. 152 (2017) 1151–1160. [PubMed: 28088460]

[174]. Salkho NM, Turki RZ, Guessoum O, Martins AM, Vitor RF, Husseini GA, Liposomes as a promising ultrasound-triggered drug delivery system in cancer treatment, Curr. Mol. Med 17 (2017) 668–688. [PubMed: 29663885]

[175]. Sennoga CA, Kanbar E, Auboire L, Dujardin P-A, Fouan D, Escoffre J-M, Bouakaz A, Microbubble-mediated ultrasound drug-delivery and therapeutic monitoring, Expert Opin. Drug Deliv 14 (2017) 1031–1043. [PubMed: 27892760]

[176]. Li X, Sui Z, Li X, Xu W, Guo Q, Sun J, Jing F, Perfluorooctylbromide nanoparticles for ultrasound imaging and drug delivery, Int. J. Nanomedicine 13 (2018) 3053. [PubMed: 29872293]

[177]. Mullick Chowdhury S, Lee T, Willmann JK, Ultrasound-guided drug delivery in cancer, Ultrasonography. 36 (2017) 171–184. doi:10.14366/usg.17021. [PubMed: 28607323]

[178]. Brigger I, Dubernet C, Couvreur P, Nanoparticles in cancer therapy and diagnosis, Adv. Drug Deliv. Rev 64 (2012) 24–36.

[179]. Hasanzadeh H, Mokhtari-Dizaji M, Bathaie SZ, Hassan ZM, Effect of local dual frequency sonication on drug distribution from polymeric nanomicelles, Ultrason. Sonochem 18 (2011) 1165–1171. [PubMed: 21489850]

[180]. Sirsi SR, Fung C, Garg S, Tianning MY, Mountford PA, Borden MA, Lung surfactant microbubbles increase lipophilic drug payload for ultrasound-targeted delivery, Theranostics. 3 (2013) 409. [PubMed: 23781287]

[181]. Chen J, Ratnayaka S, Alford A, Kozlovskaya V, Liu F, Xue B, Hoyt K, Kharlampieva E, Theranostic multilayer capsules for ultrasound imaging and guided drug delivery, ACS Nano. 11 (2017) 3135–3146. [PubMed: 28263564]

Author Manuscript Author Manuscript Author Manuscript Author Manuscript

[182]. Jain A, Tiwari A, Verma A, Jain SK, Ultrasound-based triggered drug delivery to tumors, Drug Deliv. Transl. Res 8 (2018) 150–164. doi:10.1007/s13346-017-0448-6. [PubMed: 29204925]

[183]. Cao Y, Chen Y, Yu T, Guo Y, Liu F, Yao Y, Li P, Wang D, Wang Z, Chen Y, Drug release from phase-changeable nanodroplets triggered by low-intensity focused ultrasound, Theranostics. 8 (2018) 1327. [PubMed: 29507623]

[184]. Jin H, Tan H, Zhao L, Sun W, Zhu L, Sun Y, Hao H, Xing H, Liu L, Qu X, Ultrasound-triggered thrombolysis using urokinase-loaded nanogels, Int. J. Pharm 434 (2012) 384–390. [PubMed: 22683455]

[185]. Kim J, DeRuiter R, Durham P, Tsuruta J, Goel L, Jiang X, Xu Z, Dayton PA, Perfluorocarbon nanodroplets versus microbubbles in cavitation-enhanced sonothrombolysis of retracted clots, J. Acoust. Soc. Am 146 (2019) 2775.

[186]. Wang S, Guo X, Xiu W, Liu Y, Ren L, Xiao H, Yang F, Gao Y, Xu C, Wang L, Accelerating thrombolysis using a precision and clot-penetrating drug delivery strategy by nanoparticle-shelled microbubbles, Sci. Adv 6 (2020) eaaz8204. [PubMed: 32832678]

[187]. Thein M, Cheng A, Khanna P, Zhang C, Park E-J, Ahmed D, Goodrich CJ, Asphahani F, Wu F, Smith NB, Site-specific sonoporation of human melanoma cells at the cellular level using high lateral-resolution ultrasonic micro-transducer arrays, Biosens. Bioelectron 27 (2011) 25–33. [PubMed: 21783355]

[188]. Figueiredo M, Esenaliev R, PLGA nanoparticles for ultrasound-mediated gene delivery to solid tumors, J. Drug Deliv 2012 (2012).

[189]. Zhou Q-L, Chen Z-Y, Wang Y-X, Yang F, Lin Y, Liao Y-Y, Ultrasound-mediated local drug and gene delivery using nanocarriers, Biomed Res. Int 2014 (2014).

[190]. Negishi Y, Endo-Takahashi Y, Maruyama K, Gene delivery systems by the combination of lipid bubbles and ultrasound, Drug Discov. Ther (2016).

[191]. Di J, Price J, Gu X, Jiang X, Jing Y, Gu Z, Ultrasound-triggered regulation of blood glucose levels using injectable nano-network, Adv. Healthc. Mater 3 (2014) 811–816. [PubMed: 24255016]

[192]. Di J, Yu J, Wang Q, Yao S, Suo D, Ye Y, Pless M, Zhu Y, Jing Y, Gu Z, Ultrasound-triggered noninvasive regulation of blood glucose levels using microgels integrated with insulin nanocapsules, Nano Res. 10 (2017) 1393–1402.

[193]. Hossen S, Hossain MK, Basher MK, Mia MNH, Rahman MT, Uddin MJ, Smart nanocarrier-based drug delivery systems for cancer therapy and toxicity studies: A review, J. Adv. Res 15 (2019) 1–18. doi:10.1016/j.jare.2018.06.005. [PubMed: 30581608]

[194]. Allen TM, Cullis PR, Liposomal drug delivery systems: from concept to clinical applications, Adv. Drug Deliv. Rev 65 (2013) 36–48. [PubMed: 23036225]

[195]. Marxer EEJ, Brüßler J, Becker A, Schümmelfeder J, Schubert R, Nimsky C, Bakowsky U, Development and characterization of new nanoscaled ultrasound active lipid dispersions as contrast agents, Eur. J. Pharm. Biopharm 77 (2011) 430–437. [PubMed: 21147221]

[196]. Becker A, Marxer E, Brüßler J, Hoormann AS, Kuhnt D, Bakowsky U, Nimsky C, Ultrasound active nanoscaled lipid formulations for thrombus lysis, Eur. J. Pharm. Biopharm 77 (2011) 424–429. [PubMed: 21168485]

[197]. Lattin JR, Pitt WG, Belnap DM, Husseini GA, Ultrasound-induced calcein release from eLiposomes, Ultrasound Med. Biol 38 (2012) 2163–2173. [PubMed: 23062373]

[198]. de la Rosa MAD, Husseini GA, Pitt WG, Comparing microbubble cavitation at 500 kHz and 70 kHz related to micellar drug delivery using ultrasound, Ultrasonics. 53 (2013) 377–386. [PubMed: 22901396]

[199]. Husseini GA, Velluto D, Kherbeck L, Pitt WG, Hubbell JA, Christensen DA, Investigating the acoustic release of doxorubicin from targeted micelles, Colloids Surfaces B Biointerfaces. 101 (2013) 153–155. [PubMed: 22796785]

[200]. Wu P, Jia Y, Qu F, Sun Y, Wang P, Zhang K, Xu C, Liu Q, Wang X, Ultrasoundresponsive polymeric micelles for sonoporation-assisted site-specific therapeutic action, ACS Appl. Mater. Interfaces 9 (2017) 25706–25716. [PubMed: 28741924]

Author Manuscript Author Manuscript Author Manuscript Author Manuscript

[201]. Sanson C, Diou O, Thevenot J, Ibarboure E, Soum A, Brûlet A, Miraux S, Thiaudière E, Tan S, Brisson A, Doxorubicin loaded magnetic polymersomes: theranostic nanocarriers for MR imaging and magneto-chemotherapy, ACS Nano. 5 (2011) 1122–1140. [PubMed: 21218795]

[202]. Néstor M-M, Kei N-PE, Guadalupe N-AM, Elisa M-ES, Adriana G-Q, David Q-G, Preparation and in vitro evaluation of poly (D, L-lactide-co-glycolide) air-filled nanocapsules as a contrast agent for ultrasound imaging, Ultrasonics. 51 (2011) 839–845. [PubMed: 21570702]

[203]. Yang P, Li D, Jin S, Ding J, Guo J, Shi W, Wang C, Stimuli-responsive biodegradable poly (methacrylic acid) based nanocapsules for ultrasound traced and triggered drug delivery system, Biomaterials. 35 (2014) 2079–2088. [PubMed: 24331704]

[204]. Chen W, Du J, Ultrasound and pH dually responsive polymer vesicles for anticancer drug delivery, Sci. Rep 3 (2013) 2162. [PubMed: 23831819]

[205]. Cavalli R, Bisazza A, Trotta M, Argenziano M, Civra A, Donalisio M, Lembo D, New chitosan nanobubbles for ultrasound-mediated gene delivery: preparation and in vitro characterization, Int. J. Nanomedicine 7 (2012) 3309. [PubMed: 22802689]

[206]. Yin T, Wang P, Li J, Zheng R, Zheng B, Cheng D, Li R, Lai J, Shuai X, Ultrasound-sensitive siRNA-loaded nanobubbles formed by hetero-assembly of polymeric micelles and liposomes and their therapeutic effect in gliomas, Biomaterials. 34 (2013) 4532–4543. [PubMed: 23522375]

[207]. Rapoport NY, Kennedy AM, Shea JE, Scaife CL, Nam K-H, Controlled and targeted tumor chemotherapy by ultrasound-activated nanoemulsions/microbubbles, J. Control. Release 138 (2009) 268–276. [PubMed: 19477208]

[208]. Thakkar D, Gupta R, Monson K, Rapoport N, Effect of ultrasound on the permeability of vascular wall to nano-emulsion droplets, Ultrasound Med. Biol 39 (2013) 1804–1811. [PubMed: 23849384]

[209]. Paris JL, Cabañas MV, Manzano M, Vallet-Regí M, Polymer-grafted mesoporous silica nanoparticles as ultrasound-responsive drug carriers, ACS Nano. 9 (2015) 11023–11033. [PubMed: 26456489]

[210]. Paris JL, Mannaris C, Cabañas MV, Carlisle R, Manzano M, Vallet-Regí M, Coussios CC, Ultrasound-mediated cavitation-enhanced extravasation of mesoporous silica nanoparticles for controlled-release drug delivery, Chem. Eng. J 340 (2018) 2–8.

[211]. Anirudhan TS, Nair AS, Temperature and ultrasound sensitive gatekeepers for the controlled release of chemotherapeutic drugs from mesoporous silica nanoparticles, J. Mater. Chem. B 6 (2018) 428–439. [PubMed: 32254522]

[212]. Paris JL, Manzano M, Cabañas MV, Vallet-Regí M, Mesoporous silica nanoparticles engineered for ultrasound-induced uptake by cancer cells, Nanoscale. 10 (2018) 6402–6408. [PubMed: 29561558]

[213]. Li X, Wang Z, Xia H, Ultrasound Reversible Response Nanocarrier Based on Sodium Alginate Modified Mesoporous Silica Nanoparticles, Front. Chem 7 (2019) 59. [PubMed: 30805332]

[214]. Manzano M, Vallet-Regí M, Ultrasound responsive mesoporous silica nanoparticles for biomedical applications, Chem. Commun 55 (2019) 2731–2740.

[215]. Xia Y, Li W, Cobley CM, Chen J, Xia X, Zhang Q, Yang M, Cho EC, Brown PK, Gold nanocages: from synthesis to theranostic applications, Acc. Chem. Res 44 (2011) 914–924. [PubMed: 21528889]

[216]. Xia X, Xia Y, Gold nanocages as multifunctional materials for nanomedicine, Front. Phys 9 (2014) 378–384.

[217]. Zangabad PS, Karimi M, Mehdizadeh F, Malekzad H, Ghasemi A, Bahrami S, Zare H, Moghoofei M, Hekmatmanesh A, Hamblin MR, Nanocaged platforms: modification, drug delivery and nanotoxicity. Opening synthetic cages to release the tiger, Nanoscale. 9 (2017) 1356–1392. [PubMed: 28067384]

[218]. Yang H-W, Hua M-Y, Liu H-L, Huang C-Y, Wei K-C, Potential of magnetic nanoparticles for targeted drug delivery, Nanotechnol. Sci. Appl 5 (2012) 73. [PubMed: 24198498]

[219]. V Mody V, Cox A, Shah S, Singh A, Bevins W, Parihar H, Magnetic nanoparticle drug delivery systems for targeting tumor, Appl. Nanosci 4 (2014) 385–392.

Author Manuscript Author Manuscript Author Manuscript Author Manuscript

[220]. Lee JY, Crake C, Teo B, Carugo D, de Saint Victor M, Seth A, Stride E, Ultrasound-Enhanced siRNA Delivery Using Magnetic Nanoparticle-Loaded Chitosan-Deoxycholic Acid Nanodroplets, Adv. Healthc. Mater 6 (2017) 1601246.

[221]. Chen D, Dougherty CA, Zhu K, Hong H, Theranostic applications of carbon nanomaterials in cancer: Focus on imaging and cargo delivery, J. Control. Release 210 (2015) 230–245. [PubMed: 25910580]

[222]. Al Faraj A, Shaik AP, Shaik AS, Magnetic single-walled carbon nanotubes as efficient drug delivery nanocarriers in breast cancer murine model: noninvasive monitoring using diffusion-weighted magnetic resonance imaging as sensitive imaging biomarker, Int. J. Nanomedicine 10 (2015) 157. [PubMed: 25565811]

[223]. Beg S, Rahman M, Jain A, Saini S, Hasnain MS, Swain S, Imam S, Kazmi I, Akhter S, Emergence in the functionalized carbon nanotubes as smart nanocarriers for drug delivery applications, in: Fullerens, Graphenes Nanotub, Elsevier, 2018: pp. 105–133.

[224]. Kaur J, Gill GS, Jeet K, Applications of carbon nanotubes in drug delivery: a comprehensive review, in: Charact. Biol. Nanomater. Drug Deliv, Elsevier, 2019: pp. 113–135.

[225]. Miller DL, Smith NB, Bailey MR, Czarnota GJ, Hynynen K, Makin IRS, Overview of Therapeutic Ultrasound Applications and Safety Considerations, J. Ultrasound Med 31 (2012) 623–634. doi:10.7863/jum.2012.31.4.623. [PubMed: 22441920]

[226]. Liu T, Zhang N, Wang Z, Wu M, Chen Y, Ma M, Chen H, Shi J, Endogenous catalytic generation of O2 bubbles for in situ ultrasound-guided high intensity focused ultrasound ablation, ACS Nano. 11 (2017) 9093–9102. [PubMed: 28796487]

[227]. Qian X, Zheng Y, Chen Y, Micro/nanoparticle-augmented sonodynamic therapy (SDT): Breaking the depth shallow of photoactivation, Adv. Mater 28 (2016) 8097–8129. [PubMed: 27384408]

[228]. Yang C, Li Y, Du M, Chen Z, Recent advances in ultrasound-triggered therapy, J. Drug Target 27 (2019) 33–50. [PubMed: 29659307]

[229]. Shi J, Kantoff PW, Wooster R, Farokhzad OC, Cancer nanomedicine: progress, challenges and opportunities, Nat. Rev. Cancer 17 (2017) 20. [PubMed: 27834398]

[230]. Zhou L-Q, Li P, Cui X-W, Dietrich CF, Ultrasound nanotheranostics in fighting cancer: Advances and prospects, Cancer Lett. 470 (2020) 204–219. [PubMed: 31790760]

[231]. Yang W, Lyu Q, Zhao J, Cao L, Hao Y, Zhang H, Recent advance in near-infrared/ultrasound-sensitive 2D-nanomaterials for cancer therapeutics, Sci. China Mater (2020) 1–32. [PubMed: 32219007]

[232]. Fan W, Yung B, Huang P, Chen X, Nanotechnology for multimodal synergistic cancer therapy, Chem. Rev 117 (2017) 13566–13638. [PubMed: 29048884]

[233]. Xu H, Zhang X, Han R, Yang P, Ma H, Song Y, Lu Z, Yin W, Wu X, Wang H, Nanoparticles in sonodynamic therapy: state of the art review, RSC Adv. 6 (2016) 50697–50705.

[234]. Unga J, Hashida M, Ultrasound induced cancer immunotherapy, Adv. Drug Deliv. Rev 72 (2014) 144–153. [PubMed: 24680708]

[235]. Goldhaber SZ, Bounameaux H, Pulmonary embolism and deep vein thrombosis, Lancet. 379 (2012) 1835–1846. [PubMed: 22494827]

[236]. Goel L, Jiang X, Advances in Sonothrombolysis Techniques Using Piezoelectric Transducers, Sensors. 20 (2020) 1288.

[237]. Kim J, Lindsey BD, Chang W-Y, Dai X, Stavas JM, Dayton PA, Jiang X, Intravascular forward-looking ultrasound transducers for microbubble-mediated sonothrombolysis, Sci. Rep 7 (2017) 1–10. [PubMed: 28127051]

[238]. Zhang X, Owens GE, Cain CA, Gurm HS, Macoskey J, Xu Z, Histotripsy thrombolysis on retracted clots, Ultrasound Med. Biol 42 (2016) 1903–1918. [PubMed: 27166017]

[239]. Goel L, Wu H, Zhang B, Kim J, Dayton PA, Xu Z, Jiang X, Nanodroplet-Mediated Intravascular Sonothrombolysis: Cavitation Study, in: 2020 IEEE 20th Int. Conf. Nanotechnol, IEEE, 2020: pp. 185–188.

[240]. Kim J, DeRuiter RM, Goel L, Xu Z, Jiang X, Dayton PA, A Comparison of Sonothrombolysis in Aged Clots between Low-Boiling-Point Phase-Change Nanodroplets and Microbubbles of the Same Composition, Ultrasound Med. Biol 46 (2020) 3059–3068. [PubMed: 32800631]

Author Manuscript Author Manuscript Author Manuscript Author Manuscript

[241]. Kim J, Goel L, Jiang X, Xu Z, Dayton PA, Cavitation-Enhanced High-Pressure Pulsed Sonothrombolysis with Perfluorocarbon Nanodroplets versus Microbubbles in Contracted and Uncontracted Clots, in: 2020 IEEE Int. Ultrason. Symp, IEEE, 2020: pp. 1–4.

[242]. Goel L, Wu H, Zhang B, Kim J, Dayton P, Xu Z, Jiang X, Nanodroplet Mediated Intravascular Sonothrombolysis of Retracted Clots, in: 2020 IEEE Int. Ultrason. Symp, IEEE, 2020: pp. 1–3.

[243]. Gao Y, Chan CU, Gu Q, Lin X, Zhang W, Yeo DCL, Alsema AM, Arora M, Chong MSK, Shi P, Controlled nanoparticle release from stable magnetic microbubble oscillations, NPG Asia Mater. 8 (2016) e260–e260.

[244]. Zhang B, Jiang X, Wu H, Ultrasound Thrombolysis with Magnetic Microbubbles Under a Rotational Magnetic Field, in: 2018 IEEE 13th Nanotechnol. Mater. Devices Conf, IEEE, 2018: pp. 1–4.

[245]. Zhang B, Kim H, Wu H, Gao Y, Jiang X, Sonothrombolysis with magnetic microbubbles under a rotational magnetic field, Ultrasonics. 98 (2019) 62–71. [PubMed: 31202970]

[246]. Shangguan H, Casperson LW, Shearin A, Gregory KW, Prahl SA, Photoacoustic drug delivery: The effect of laser parameters on the spatial distribution of delivered drug, in: Laser-Tissue Interact. VI, International Society for Optics and Photonics, 1995: pp. 394–403.

[247]. Shangguan H, Casperson LW, Shearin A, Prahl SA, Investigation of cavitation bubble dynamics using particle image velocimetry: Implications for photoacoustic drug delivery, in: Lasers Surg. Adv. Charact. Ther. Syst. VI, International Society for Optics and Photonics, 1996: pp. 104–116.

[248]. Di J, Kim J, Hu Q, Jiang X, Gu Z, Spatiotemporal drug delivery using laser-generated-focused ultrasound system, J. Control. Release 220 (2015) 592–599. [PubMed: 26299506]

[249]. Ray PC, Khan SA, Singh AK, Senapati D, Fan Z, Nanomaterials for targeted detection and photothermal killing of bacteria, Chem. Soc. Rev 41 (2012) 3193–3209. [PubMed: 22331210]

[250]. Rai P, Mallidi S, Zheng X, Rahmanzadeh R, Mir Y, Elrington S, Khurshid A, Hasan T, Development and applications of photo-triggered theranostic agents, Adv. Drug Deliv. Rev 62 (2010) 1094–1124. [PubMed: 20858520]

[251]. Fomina N, Sankaranarayanan J, Almutairi A, Photochemical mechanisms of light-triggered release from nanocarriers, Adv. Drug Deliv. Rev 64 (2012) 1005–1020. [PubMed: 22386560]

[252]. Cheng L, He W, Gong H, Wang C, Chen Q, Cheng Z, Liu Z, PEGylated micelle nanoparticles encapsulating a non-fluorescent near-infrared organic dye as a safe and highly-effective photothermal agent for in vivo cancer therapy, Adv. Funct. Mater 23 (2013) 5893–5902.

[253]. Sivasubramanian K, Mathiyazhakan M, Wiraja C, Upputuri PK, Xu C, Pramanik M, Near-infrared light-responsive liposomal contrast agent for photoacoustic imaging and drug release applications, J. Biomed. Opt 22 (2016) 41007.

[254]. Zhang L, Gao S, Zhang F, Yang K, Ma Q, Zhu L, Activatable hyaluronic acid nanoparticle as a theranostic agent for optical/photoacoustic image-guided photothermal therapy, ACS Nano. 8 (2014) 12250–12258. [PubMed: 25402600]

[255]. Wang Y, Strohm EM, Sun Y, Wang Z, Zheng Y, Wang Z, Kolios MC, Biodegradable polymeric nanoparticles containing gold nanoparticles and Paclitaxel for cancer imaging and drug delivery using photoacoustic methods, Biomed. Opt. Express 7 (2016) 4125–4138. [PubMed: 27867720]

[256]. Shi S, Liu Y, Chen Y, Zhang Z, Ding Y, Wu Z, Yin J, Nie L, Versatile pH-response micelles with high cell-penetrating helical diblock copolymers for photoacoustic imaging guided synergistic chemo-photothermal therapy, Theranostics. 6 (2016) 2170. [PubMed: 27924155]

[257]. Liu X, Yang G, Zhang L, Liu Z, Cheng Z, Zhu X, Photosensitizer cross-linked nano-micelle platform for multimodal imaging guided synergistic photothermal/photodynamic therapy, Nanoscale. 8 (2016) 15323–15339. [PubMed: 27503666]

[258]. Guo M, Mao H, Li Y, Zhu A, He H, Yang H, Wang Y, Tian X, Ge C, Peng Q, Dual imaging-guided photothermal/photodynamic therapy using micelles, Biomaterials. 35 (2014) 4656–4666. [PubMed: 24613048]

[259]. Gong H, Dong Z, Liu Y, Yin S, Cheng L, Xi W, Xiang J, Liu K, Li Y, Liu Z, Engineering of multifunctional nanomicelles for combined photothermal and photodynamic therapy under the guidance of multimodal imaging, Adv. Funct. Mater 24 (2014) 6492–6502.

Author Manuscript Author Manuscript Author Manuscript Author Manuscript

[260]. Wang T, Wang D, Yu H, Wang M, Liu J, Feng B, Zhou F, Yin Q, Zhang Z, Huang Y, Intracellularly acid-switchable multifunctional micelles for combinational photo/chemotherapy of the drug-resistant tumor, ACS Nano. 10 (2016) 3496–3508. [PubMed: 26866752]

[261]. Cai Y, Liang P, Tang Q, Yang X, Si W, Huang W, Zhang Q, Dong X, Diketopyrrolopyrrole–triphenylamine organic nanoparticles as multifunctional reagents for photoacoustic imaging-guided photodynamic/photothermal synergistic tumor therapy, ACS Nano. 11 (2017) 1054–1063. [PubMed: 28033465]

[262]. Zhang J, Yang C, Zhang R, Chen R, Zhang Z, Zhang W, Peng S, Chen X, Liu G, Hsu C, Biocompatible D–A Semiconducting Polymer Nanoparticle with LightHarvesting Unit for Highly Effective Photoacoustic Imaging Guided Photothermal Therapy, Adv. Funct. Mater 27 (2017) 1605094. [PubMed: 29046623]

[263]. Fan Q, Cheng K, Hu X, Ma X, Zhang R, Yang M, Lu X, Xing L, Huang W, Gambhir SS, Transferring biomarker into molecular probe: melanin nanoparticle as a naturally active platform for multimodality imaging, J. Am. Chem. Soc 136 (2014) 15185–15194. [PubMed: 25292385]

[264]. Zhang R, Fan Q, Yang M, Cheng K, Lu X, Zhang L, Huang W, Cheng Z, Engineering melanin nanoparticles as an efficient drug–delivery system for imaging-guided chemotherapy, Adv. Mater 27 (2015) 5063–5069. [PubMed: 26222210]

[265]. Chen J, Yang M, Zhang Q, Cho EC, Cobley CM, Kim C, Glaus C, V Wang L, Welch MJ, Xia Y, Gold nanocages: a novel class of multifunctional nanomaterials for theranostic applications, Adv. Funct. Mater 20 (2010) 3684–3694. [PubMed: 33907543]

[266]. Manivasagan P, Bharathiraja S, Bui NQ, Lim IG, Oh J, Paclitaxel-loaded chitosan oligosaccharide-stabilized gold nanoparticles as novel agents for drug delivery and photoacoustic imaging of cancer cells, Int. J. Pharm 511 (2016) 367–379. [PubMed: 27424169]

[267]. Huang P, Lin J, Li W, Rong P, Wang Z, Wang S, Wang X, Sun X, Aronova M, Niu G, Biodegradable gold nanovesicles with an ultrastrong plasmonic coupling effect for photoacoustic imaging and photothermal therapy, Angew. Chemie Int. Ed 52 (2013) 13958–13964.

[268]. Wilson K, Homan K, Emelianov S, Biomedical photoacoustics beyond thermal expansion using triggered nanodroplet vaporization for contrast-enhanced imaging, Nat. Commun 3 (2012) 618. [PubMed: 22233628]

[269]. Zhong J, Yang S, Wen L, Xing D, Imaging-guided photoacoustic drug release and synergistic chemo-photoacoustic therapy with paclitaxel-containing nanoparticles, J. Control. Release 226 (2016) 77–87. [PubMed: 26860283]

[270]. Duan S, Yang Y, Zhang C, Zhao N, Xu F, NIR-Responsive Polycationic Gatekeeper-Cloaked Hetero-Nanoparticles for Multimodal Imaging-Guided Triple-Combination Therapy of Cancer, Small. 13 (2017) 1603133.

[271]. Huang L, Ao L, Hu D, Wang W, Sheng Z, Su W, Magneto-plasmonic nanocapsules for multimodal-imaging and magnetically guided combination cancer therapy, Chem. Mater 28 (2016) 5896–5904.

[272]. Fu G, Liu W, Feng S, Yue X, Prussian blue nanoparticles operate as a new generation of photothermal ablation agents for cancer therapy, Chem. Commun 48 (2012) 11567–11569.

[273]. Liang X, Deng Z, Jing L, Li X, Dai Z, Li C, Huang M, Prussian blue nanoparticles operate as a contrast agent for enhanced photoacoustic imaging, Chem. Commun 49 (2013) 11029–11031.

[274]. Jing L, Liang X, Deng Z, Feng S, Li X, Huang M, Li C, Dai Z, Prussian blue coated gold nanoparticles for simultaneous photoacoustic/CT bimodal imaging and photothermal ablation of cancer, Biomaterials. 35 (2014) 5814–5821. [PubMed: 24746962]

[275]. Cheng L, Gong H, Zhu W, Liu J, Wang X, Liu G, Liu Z, PEGylated Prussian blue nanocubes as a theranostic agent for simultaneous cancer imaging and photothermal therapy, Biomaterials. 35 (2014) 9844–9852. [PubMed: 25239041]

[276]. Cai X, Jia X, Gao W, Zhang K, Ma M, Wang S, Zheng Y, Shi J, Chen H, A Versatile Nanotheranostic Agent for Efficient Dual-Mode Imaging Guided Synergistic Chemo-Thermal Tumor Therapy, Adv. Funct. Mater 25 (2015) 2520–2529.

[277]. Chen W, Zeng K, Liu H, Ouyang J, Wang L, Liu Y, Wang H, Deng L, Liu Y, Cell membrane camouflaged hollow prussian blue nanoparticles for synergistic photothermal-/chemotherapy of cancer, Adv. Funct. Mater 27 (2017) 1605795.

Author Manuscript Author Manuscript Author Manuscript Author Manuscript

[278]. Bao T, Yin W, Zheng X, Zhang X, Yu J, Dong X, Yong Y, Gao F, Yan L, Gu Z, One-pot synthesis of PEGylated plasmonic MoO3–x hollow nanospheres for photoacoustic imaging guided chemo-photothermal combinational therapy of cancer, Biomaterials. 76 (2016) 11–24. [PubMed: 26517561]

[279]. Song X, Wang X, Yu S, Cao J, Li S, Li J, Liu G, Yang H, Chen X, Co9Se8 Nanoplates as a New Theranostic Platform for Photoacoustic/Magnetic Resonance Dual-Modal-Imaging-Guided Chemo-Photothermal Combination Therapy, Adv. Mater 27 (2015) 3285–3291. [PubMed: 25885638]

[280]. Sheng Z, Song L, Zheng J, Hu D, He M, Zheng M, Gao G, Gong P, Zhang P, Ma Y, Protein-assisted fabrication of nano-reduced graphene oxide for combined in vivo photoacoustic imaging and photothermal therapy, Biomaterials. 34 (2013) 5236–5243. [PubMed: 23602365]

[281]. Kim J, Chang W-Y, Lindsey BD, Dayton PA, Dai X, Stavas JM, Jiang X, Laser-generated-focused ultrasound transducers for microbubble-mediated, dual-excitation sonothrombolysis, in: 2016 IEEE Int. Ultrason. Symp, IEEE, 2016: pp. 1–4.

[282]. Wu H, Kim H, Tang Y, Yao J, Jiang X, Fiber-optic laser-ultrasound transducer using carbon nanoparticles for intravascular sonothrombolysis, in: 2019 IEEE 19th Int. Conf. Nanotechnol, IEEE, 2019: pp. 261–264.

[283]. Wu H, Tang Y, Kim H, Yao J, Jiang X, Fiber based laser ultrasound transducer for intravascular thrombolysis with detective photoacoustic imaging, in: 2020 IEEE Int. Ultrason. Symp, IEEE, 2020: pp. 1–4.

Author Manuscript Author Manuscript Author Manuscript Author Manuscript

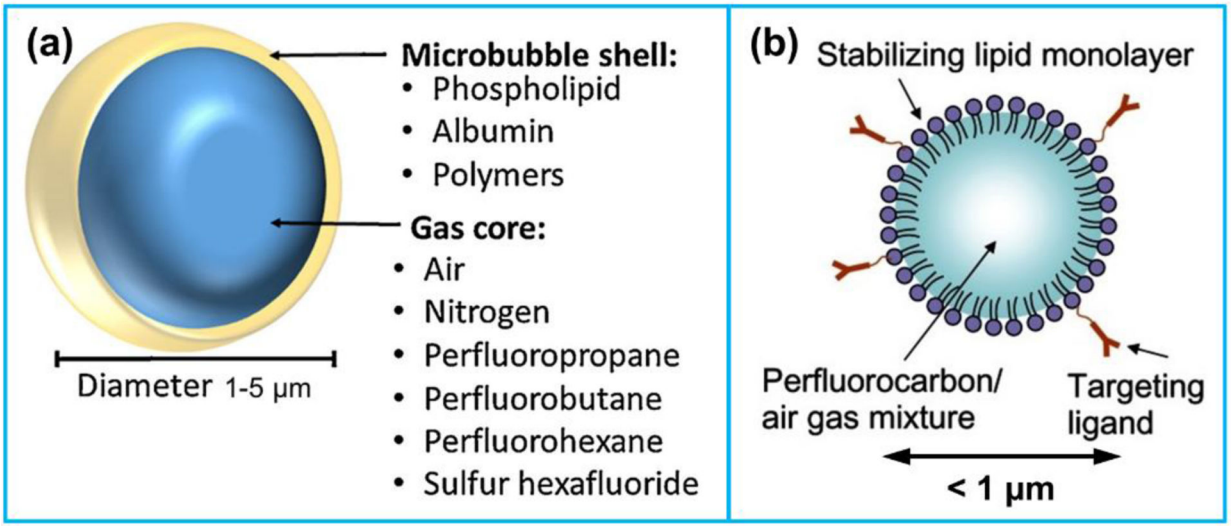

Figure 1.

(a) Structure of a microbubble. Reproduced with permission [16]. Copyright 2015, Elsevier.

(b) Composition of a nanosized ultrasound contrast agent. Reproduced with permission [19]. Copyright 2013, Dove Medical Press Ltd.

Author Manuscript Author Manuscript Author Manuscript Author Manuscript

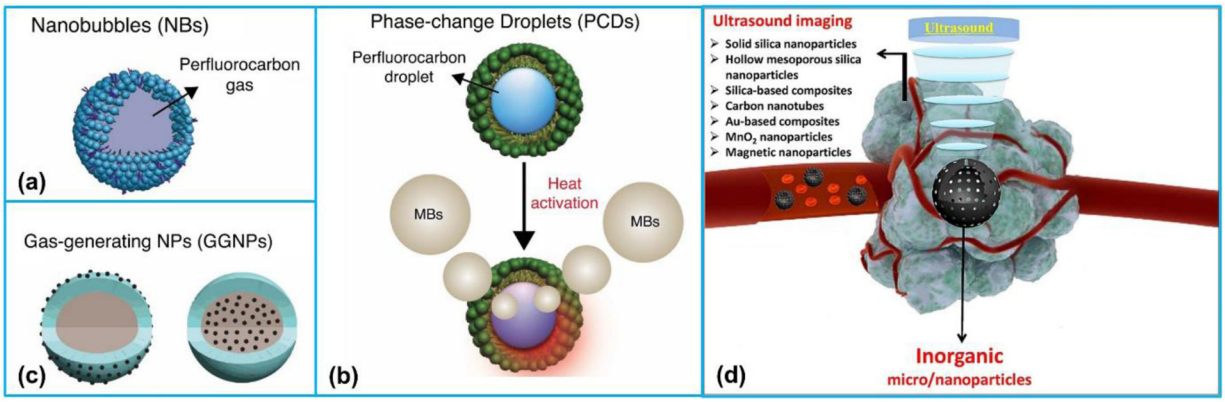

Figure 2.

Schematic representation of organic and inorganic nanosized UCAs for ultrasound imaging. Organic UCAs: (a) nanobubbles, (b) phase-change droplets, and (c) gas-generating nanoparticles. (a)-(c) Reproduced with permission [29]. Copyright 2018, Elsevier. (d) The summary of inorganic nanoparticles. Reproduced with permission [30]. Copyright 2017, Elsevier.

Author Manuscript Author Manuscript Author Manuscript Author Manuscript

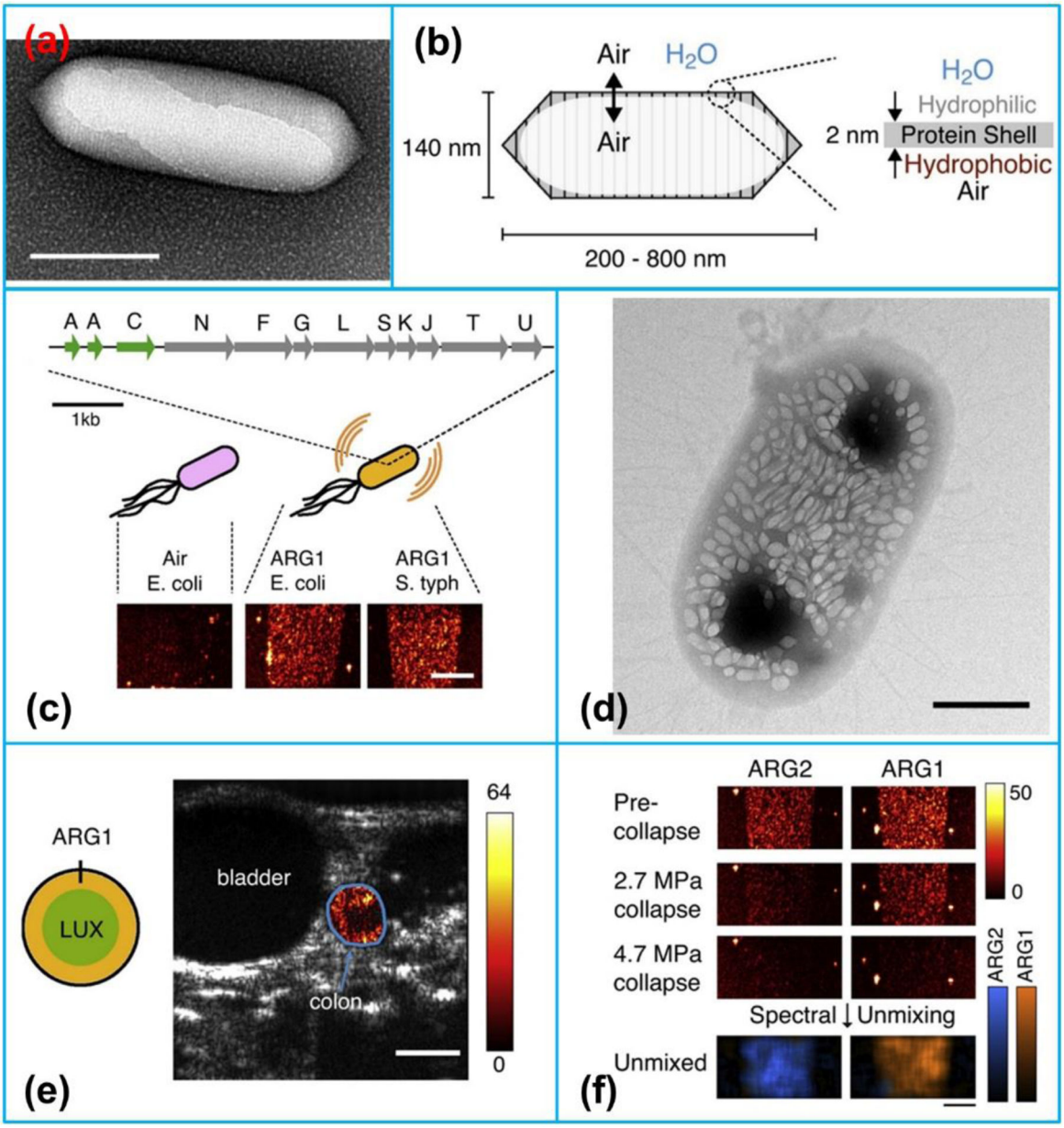

Figure 3.

(a) Transmission electron microscopy (TEM) image of a gas vesicle (scale bars, 150 nm). (b) Composition of a gas vesicle. (c) Engineered gene, ARG1, comprising genes from A. flos-aquae (green) and B. megaterium (gray) to make the gas vesicles detectable by ultrasound in heterologous host. (d) TEM image of an E. coli Nissle 1917 cell expressing ARG1 (scale bar, 50 nm). (e) Ultrasound image of a live mouse with ARG1-expressing E. coli arranged in the colon (scale bar, 2.5 mm). (f) Ultrasound images of ARG1 and ARG2 before and after the application of two different collapse pressures. Reproduced with permission [83]. Copyright 2018, Elsevier.

Author Manuscript Author Manuscript Author Manuscript Author Manuscript

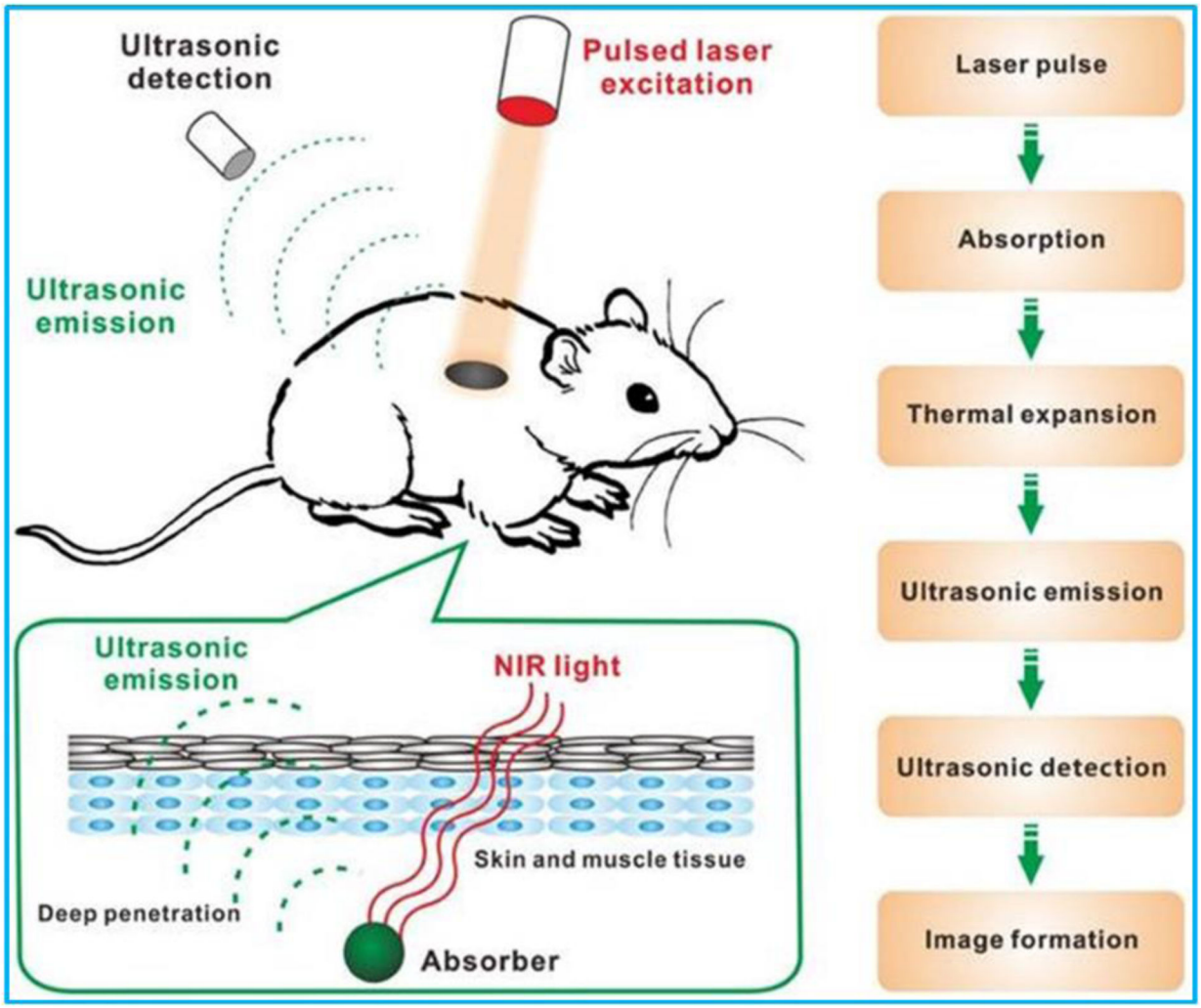

Figure 4.
Schematic of working principle of PA imaging. Reproduced with permission [85]. Copyright 2016, Ivyspring International Publisher.

Author Manuscript Author Manuscript Author Manuscript Author Manuscript

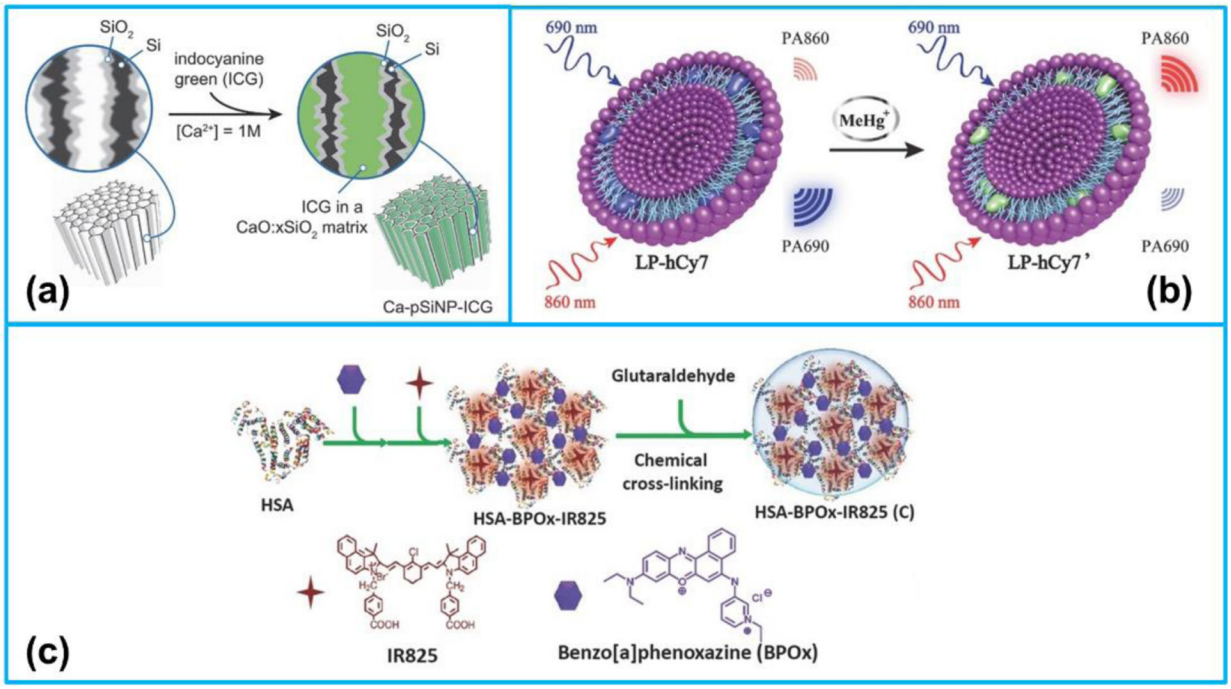

Figure 5.

(a) Procedure used to simultaneously load and seal CG into the pores of porous silicon nanoparticles (pSiNPs). Reproduced with permission [102]. Copyright 2018, Wiley-VCH. (b) Mechanism of ratiometric PA imaging of $MeHg^{+}$. Reproduced with permission [114]. Copyright 2017, Wiley-VCH. (c) The preparation process of C-HSA-BPOx-IR825. Reproduced with permission [111]. Copyright 2015, Wiley-VCH.

Author Manuscript Author Manuscript Author Manuscript Author Manuscript

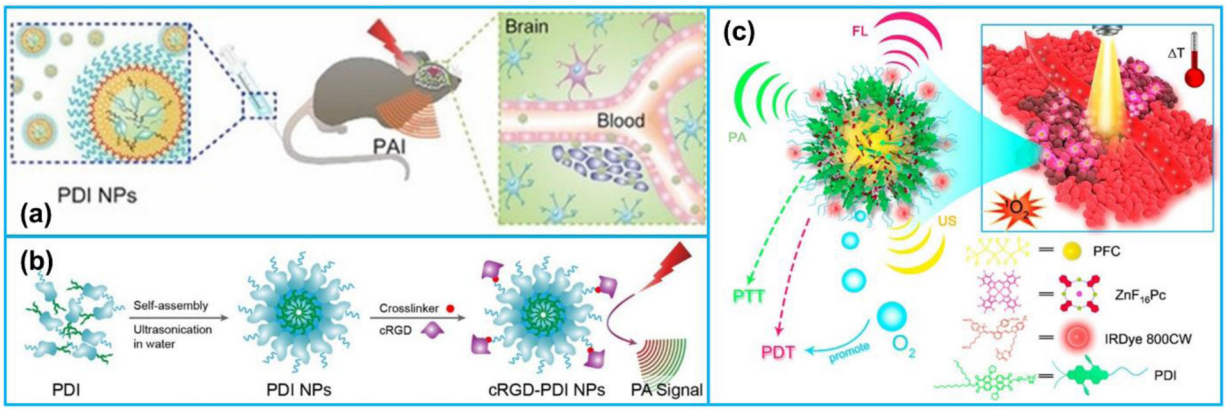

Figure 6.

(a) PA imaging process of brain tumor in vivo by PDI NPs. Reproduced with permission [98]. Copyright 2015, Wiley-VCH. (b) The preparation of cRGD-PDI NPs. Reproduced with permission [105]. Copyright 2017, American Chemical Society. (c) IRDye800CW-labeled photosensitizer $ZnF_{16}P_c$-loaded PDI photoacoustic nanodroplet (PS-PDI-PAnD). Reproduced with permission [116]. Copyright 2018, American Chemical Society.

Author Manuscript Author Manuscript Author Manuscript Author Manuscript

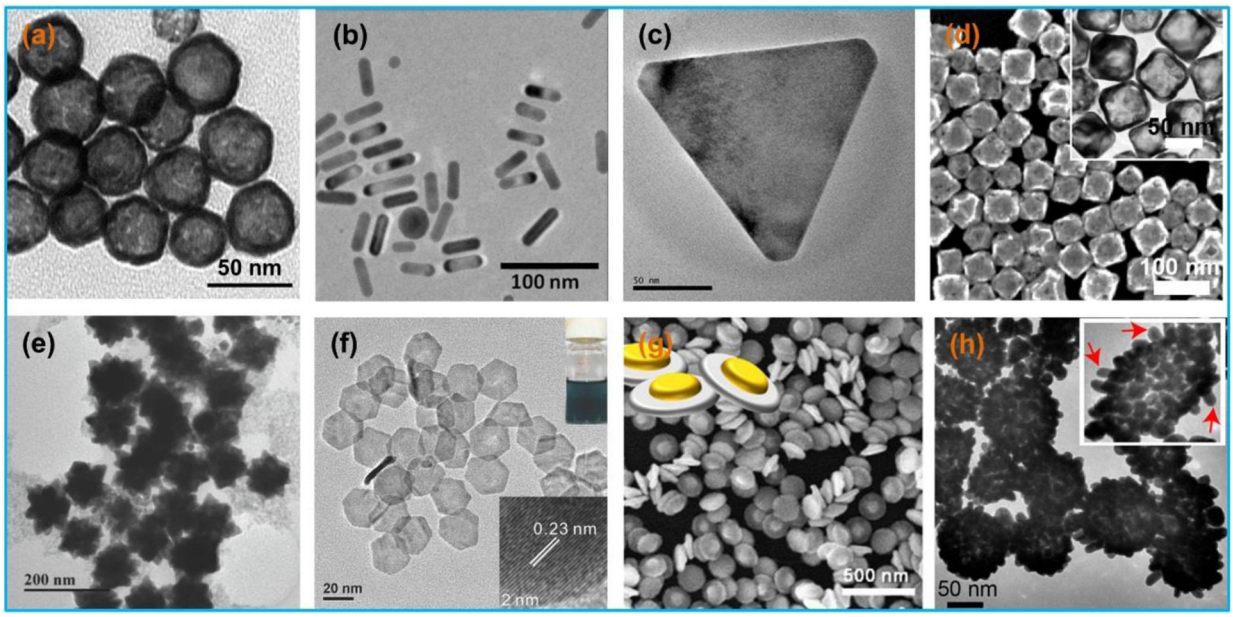

Figure 7.

Microscopy photographs of different types of gold nanoparticles: (a) nanospheres, (b) nanorods, (c) nanoprisms, (d) nanocages, (e) nanostars, (f) nanoplates, (g) nanodisks, and (h) nanoshells. (a) Reproduced with permission [148]. Copyright 2009, Elsevier. (b) Reproduced with permission [149]. Copyright 2012, American Chemical Society. (c) Reproduced with permission [126]. Copyright 2015, American Chemical Society. (d) Reproduced with permission [131]. Copyright 2017, Elsevier. (e) Reproduced with permission [150]. Copyright 2018, Wiley-VCH. (f) Reproduced with permission [135]. Copyright 2014, Wiley-VCH. (g) Reproduced with permission [139]. Copyright 2017, American Chemical Society. (h) Reproduced with permission [142]. Copyright 2017, American Chemical Society.

Author Manuscript Author Manuscript Author Manuscript Author Manuscript

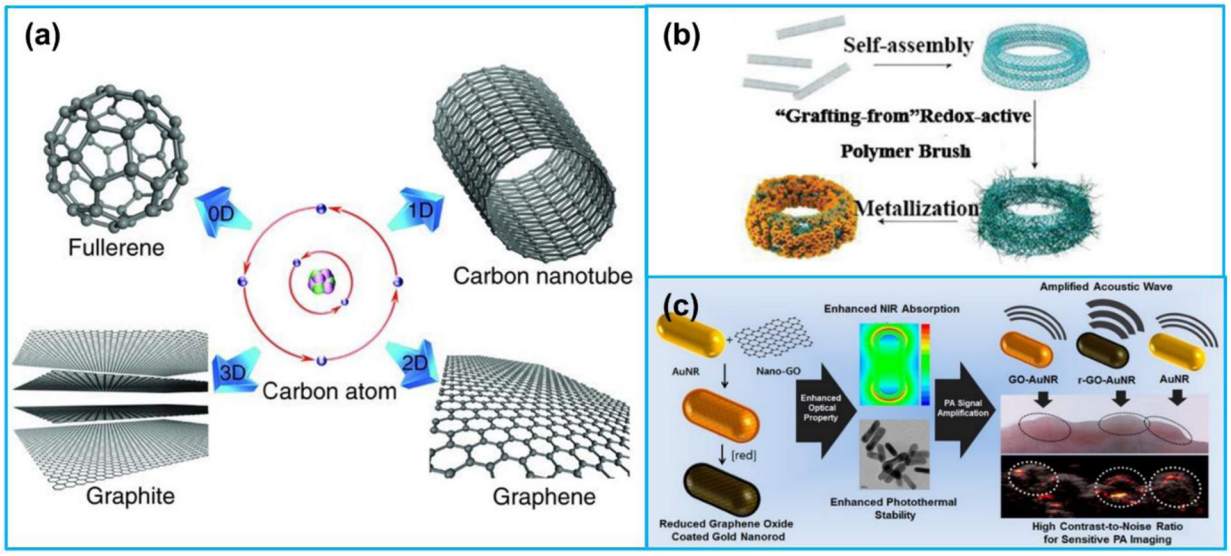

Figure 8.

(a) Structures of 0D fullerene, 1D carbon nanotube, 2D graphene and 3D graphite formed by the carbon atoms. (b) Preparation of CNT ring Au nanoparticles (CNTR @ AuNPs). (c) Preparation and application of reduced graphene oxide Au nanorods (rGO-AuNRs). (a) Reproduced with permission [167]. Copyright 2011, Wiley-VCH. (b) Reproduced with permission [164]. Copyright 2016, American Chemical Society. (c) Reproduced with permission [165]. Copyright 2015, American Chemical Society.

Author Manuscript Author Manuscript Author Manuscript Author Manuscript

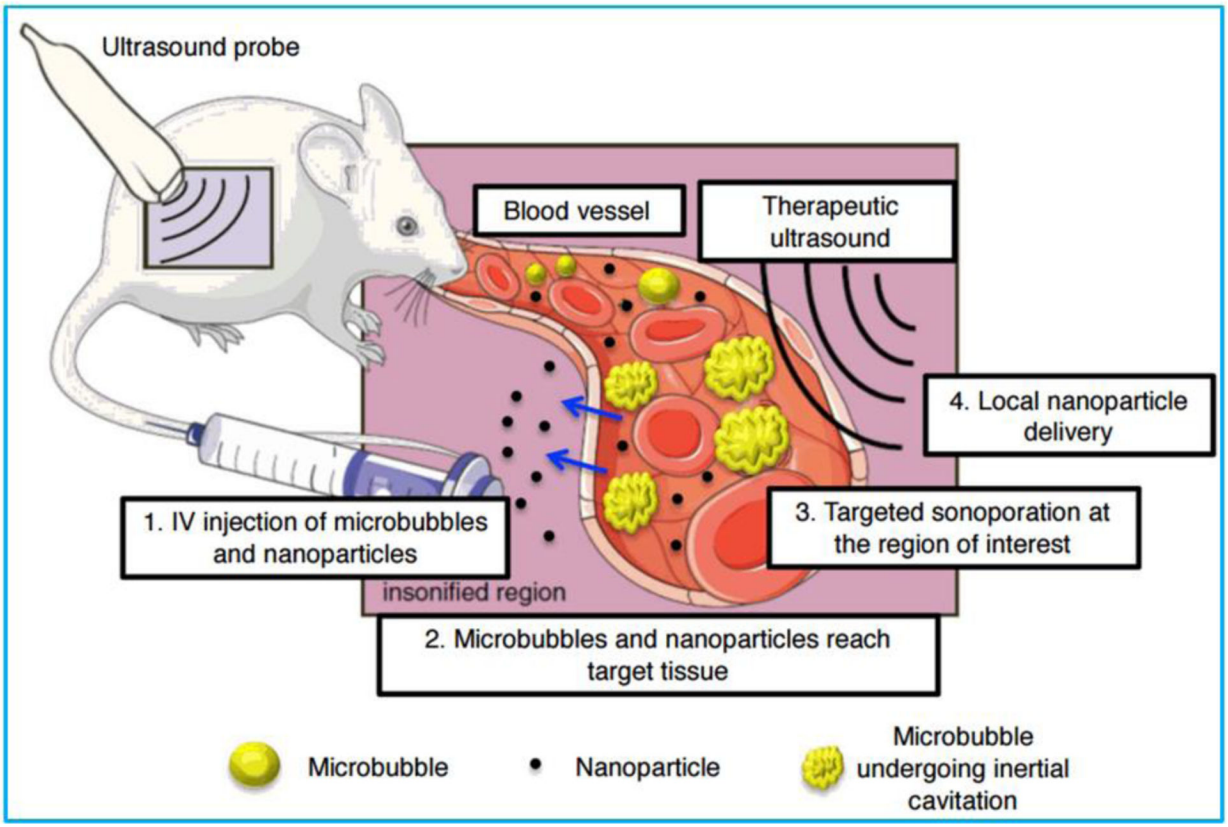

Figure 9.

Schematic illustration of the mechanism of ultrasound-mediated nanoparticle delivery. Reproduced with permission [177]. Copyright 2017, Korean Society of Ultrasound in Medicine.

Author Manuscript Author Manuscript Author Manuscript Author Manuscript

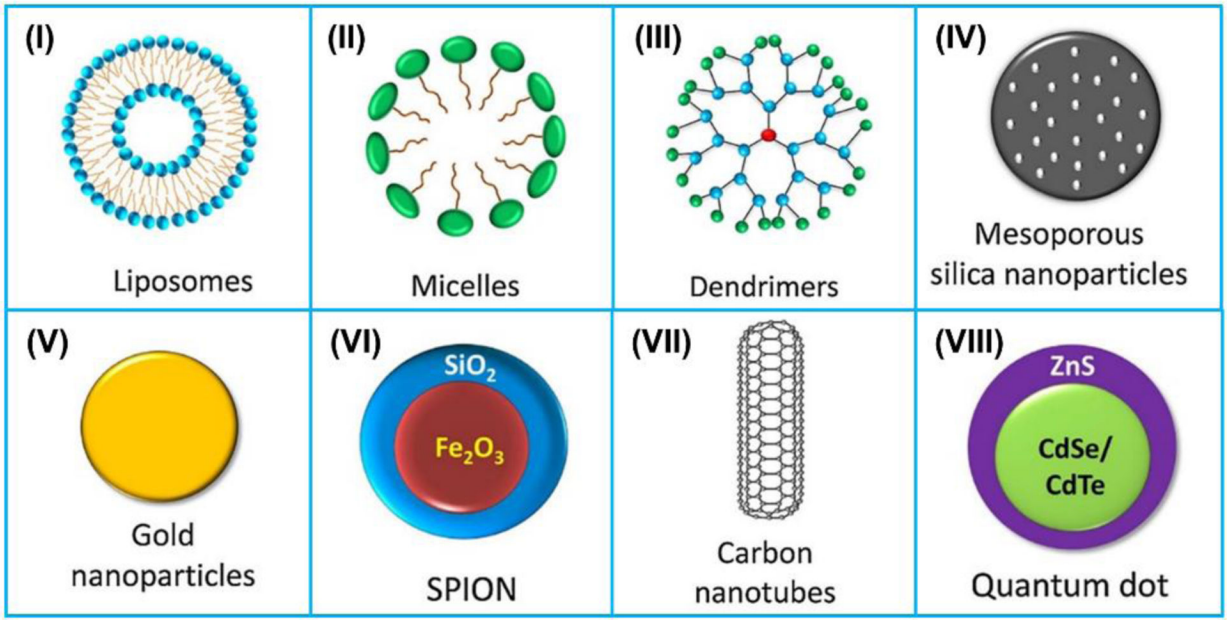

Figure 10.

Schematic illustration of the 8 most reported nanocarriers: (I) liposomes, (II) micelles, (III) dendrimers, (IV) meso-porous silica nanoparticles (MSNs), (V) gold nanoparticles (AuNPs), (VI) super paramagnetic iron oxide nanoparticles (SPIONs), (VII) carbon nanotubes (CNTs), and (VIII) quantum dots (QDs). Reproduced with permission [193]. Copyright 2019, Elsevier.

Author Manuscript Author Manuscript Author Manuscript Author Manuscript

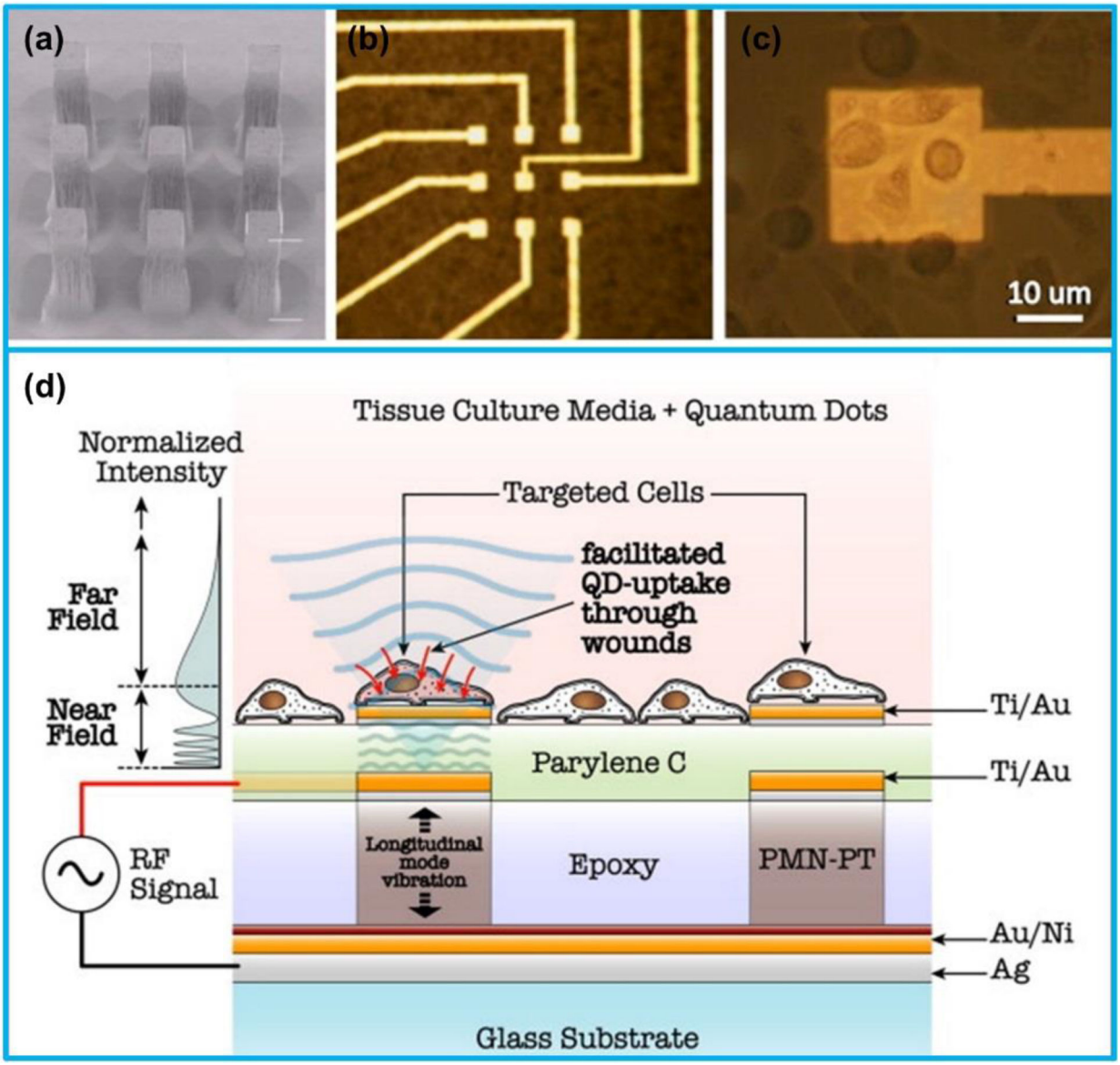

Figure 11.

(a) SEM mage of a 3 × 3 micro-transducer array (each area 25 μm × 25 μm). (b) Electrode above each micro-transducer. (c) Human melanoma cells above a micro-transducer. (d) Schematic illustration of ultrasound-mediated quantum dots (QDs) delivery at cellular level using the micro-transducer array. (a)-(d) Reproduced with permission [187]. Copyright 2011, Elsevier.

Author Manuscript Author Manuscript Author Manuscript Author Manuscript

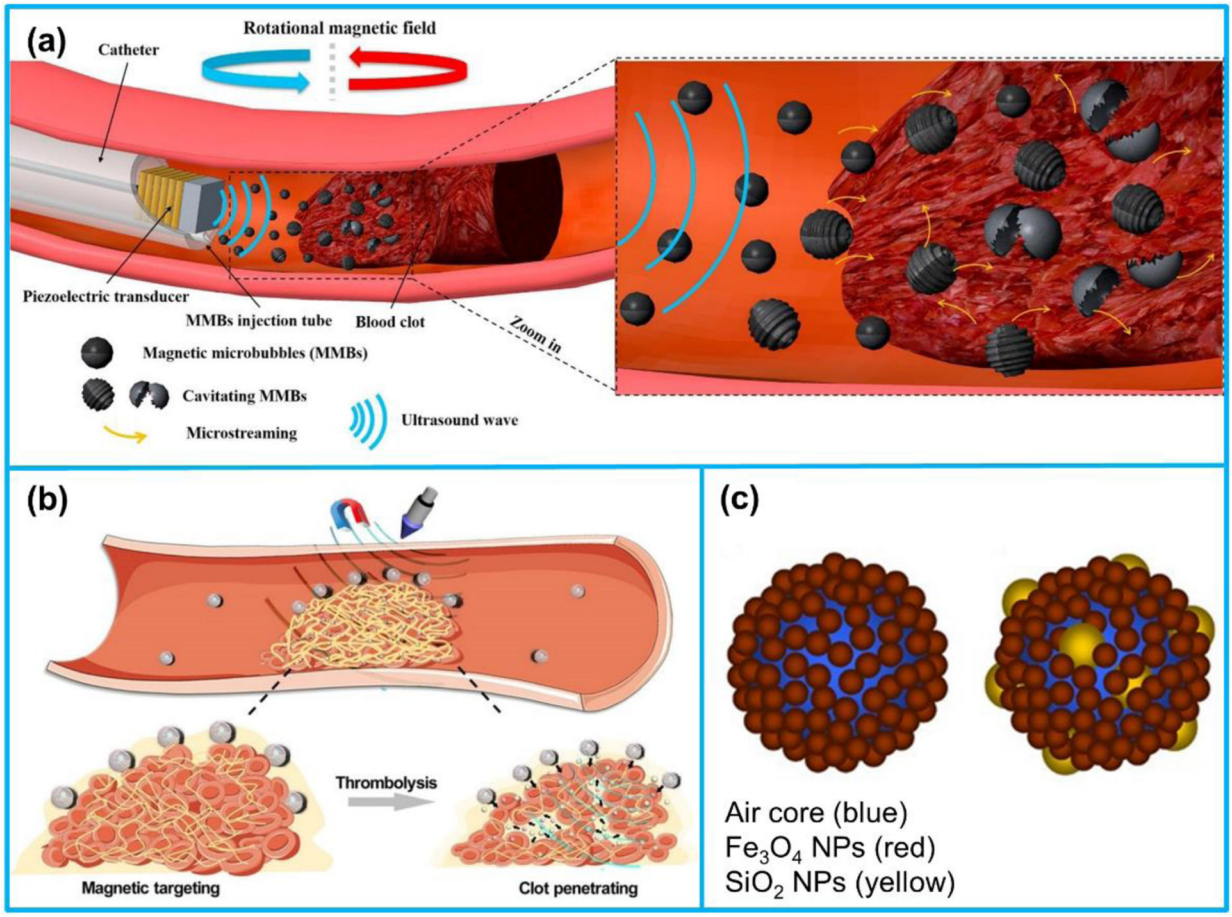

Figure 12.

(a) Illustration of magnetic microbubbles (MMBs)-mediated sonothrombolysis. (b) Schematic view of SiO_2-tPA shelled MMBs for targeted tPA delivery and controlled release. (c) Composition of MMBs. (a) Reproduced with permission [245]. Copyright 2019, Elsevier. (b) Reproduced with permission [186]. Copyright 2020, American Association for the Advancement of Science. (c) Reproduced with permission [243]. Copyright 2016, Springer Nature.

Author Manuscript Author Manuscript Author Manuscript Author Manuscript

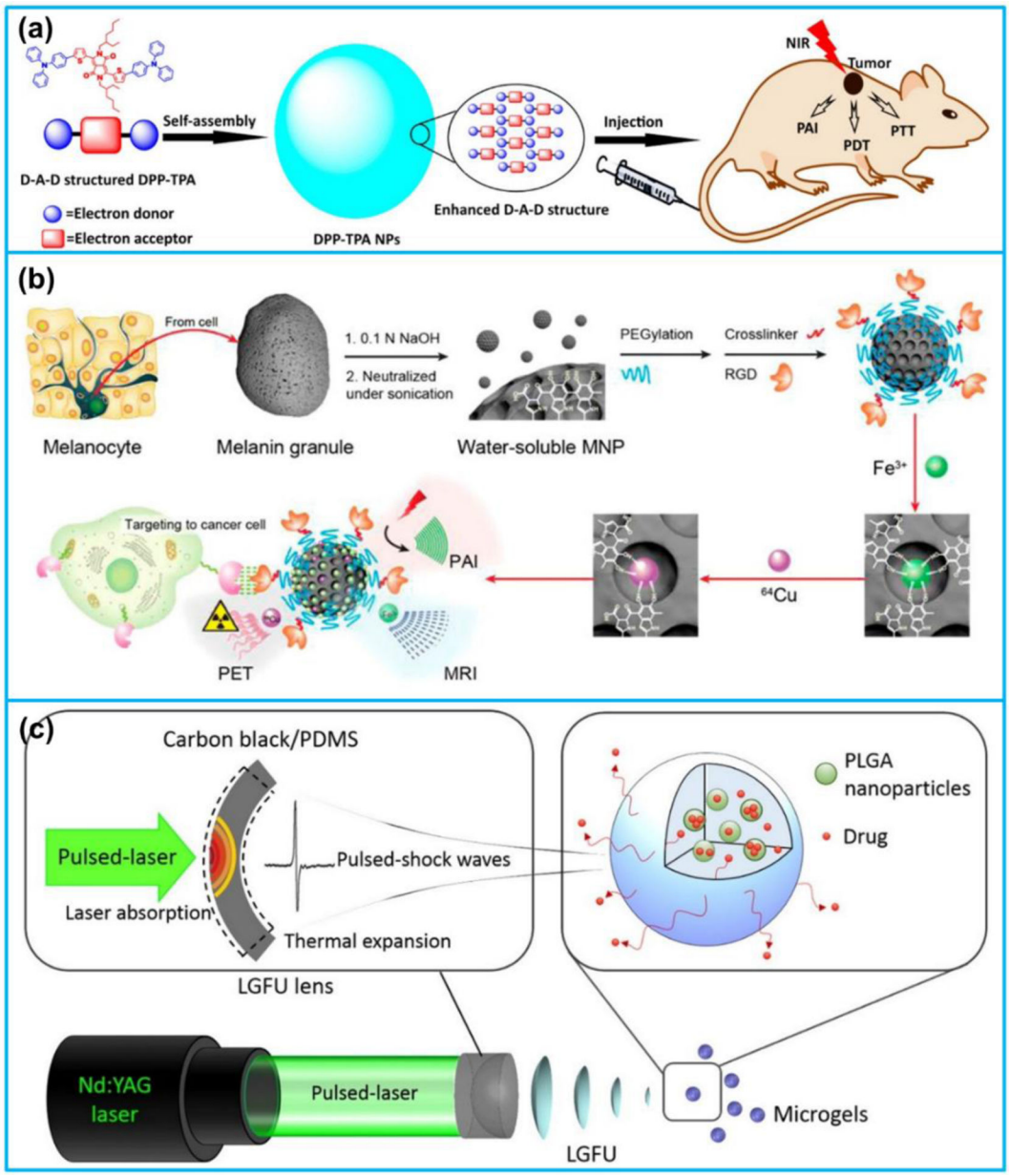

Figure 13.

(a) D-A-D structured DPP-TPA NPs as theranostic agents for PA imaging-guided PDT/PTT. (b) Multimodality molecular imaging of MNPs. (c) Laser-generated-focused ultrasound-mediated drug delivery. (a) Reproduced with permission [261]. Copyright 2017, American Chemical Society. (b) Reproduced with permission [263]. Copyright 2014, American Chemical Society. (c) Reproduced with permission [248]. Copyright 2015, Elsevier.

Author Manuscript Author Manuscript Author Manuscript Author Manuscript

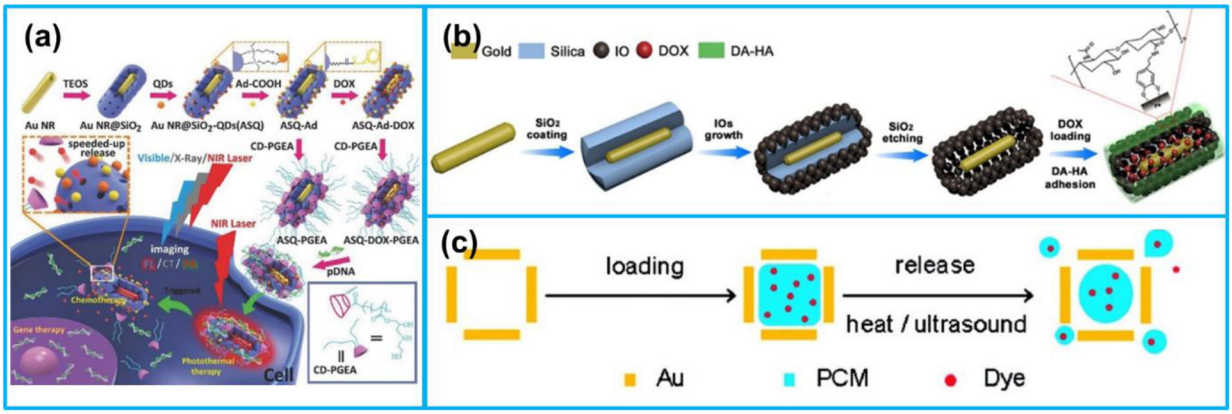

Figure 14.

(a) Preparation processes of multimodal imaging-guided therapeutic platforms. (b) Preparation of GNR @ IOs-DOX nanocapsules. (c) Loading the hollow interior of an AuNC with a dye doped PCM and then releasing t from the AuNC. (a) Reproduced with permission [270]. Copyright 2016, Wiley-VCH. (b) Reproduced with permission [271]. Copyright 2016, American Chemical Society. (c) Reproduced with permission [130]. Copyright 2011, American Chemical Society.

Author Manuscript Author Manuscript Author Manuscript Author Manuscript

Table 1.

Summary of organic nanosized UCAs for ultrasound imaging applications.

Organic nano sized UCAs	Composition	Diameter	Cytotoxicity	Applications
Nanobubbles (NBs)	NB-affibody conjugates [31]	478.2 ± 29.7 nm	No distinct cytotoxicity	Molecular ultrasound imaging of tumor
	Anti-PSMA nanobody coated nanobubbles [32]	487.60 ± 33.55 nm	N/A	Prostate cancer-targeted imaging
	Herceptin-targeted nanobubbles [33]	613.0 ± 25.4 nm	Low cytotoxicity	Diagnosis and treatment of Her-2-positive breast cancers
	CA-125 antibody-conjugated nanobubbles [34]	74.6 ± 16.7 nm	No recognizable cytotoxicity	Diagnosis of ovarian cancer
	Crosslinked pluronic-lipid-perfluorocarbon nanobubbles [35]	95.2 ± 25.2 nm	N/A	Tumor detection
Phase-change nanodroplets	Liquid core of perfluorooctyl bromide liposome conjugated with folic acid and polyethylene glycol [36]	301 ± 10.8 nm	N/A	Diagnosis of folate receptor (FR)-overexpressing tumors
	Phase changeable perfluoropentane nanodroplets [37]	321 ± 67 nm	N/A	tumor-targeted ultrasound imaging
	Diatrizoic acid conjugated glycol chitosan nanoparticles [38]	454.9 ± 3.33 nm	Having potential toxicity	Tumor diagnosis
	Oleic-acid-coated Fe_3O_4 nanoparticles [39]	294 nm	No appreciable toxicity	Tumor imaging and therapy
	Liquid perfluorohexane core encapsulated by a fluorosurfactant polymer shell [40]	180 nm	N/A	Molecular ultrasound imaging of tumor
	Perfluorohexane and carbon nanoparticles encapsulated by PLGA [41]	435.9 ± 41.31 nm	Low cytotoxicity	Sentinel lymph nodes detection and therapy of lymph nodes
	Photosensitizer and perfluorocarbon coencapsulated by lipids [42]	200 nm	No significant cytotoxicity	Photodynamic therapy
	Perfluorohexane-loaded magnetic hollow iron oxide nanoparticles [43]	537.3 nm	No distinct cytotoxicity	Stimuli-responsive cancer theranostics
	Poly lactide-glycolide acid (PLGA) nanocapsules [44]	450 nm	Negligible cytotoxicity	Cancer theranostics
	Perfluorocarbons core and lipid shell [45]	132 ± 78 nm	Low cytotoxicity	Tumor therapy
Gas-generating nanoparticles	CO_2-generating carbonate copolymer nanoparticles [46]	290 ± 18 nm	No significant cytotoxicity	Tumor-targeted US imaging and US-triggered drug delivery
	H_2O_2-triggered CO_2-generating antioxidant poly(vanillin oxalate) [47]	~550 nm	Negligible cytotoxicity	Ultrasound imaging and therapy for hepatic ischemia/reperfusion treatment
	CO_2-generating nano-lipid carriers [48]	152.4 ± 0.6	No significant cytotoxicity	Temperature-controlled drug release and multimodal imaging
	Calcium carbonate loaded alginate nanocarrier [49]	~160 nm	No appreciable toxicity	In vivo tumor imaging
	CO_2-generating mesoporous calcium carbonate (MCC) nanoparticles [50]	~250 nm	No significant cytotoxicity	Ultrasound imaging-guided cancer therapy
	Calcium carbonate encapsulated by poly(d,l-lactide-co-glycolide) [51]	220 nm	No significant cytotoxicity	Ultrasound imaging and treating neuroblastoma

Author Manuscript

Author Manuscript

Author Manuscript

Author Manuscript

Organic nano sized UCAs	Composition	Diameter	Cytotoxicity	Applications
	Doxorubicin (DOX)-loaded calcium carbonate nanoparticles [52]	240.8 ± 8.1 nm	No appreciable toxicity	Theranostic agent for cancer treatment
	Superparamagnetic iron oxide particles @ glycol chitosan nanogel [53]	218 nm	No appreciable toxicity	Dual-modality US/MR imaging
	O_2-generating hybrid ICG-HANP/ MnO2 nanocomplex [54]	239 ± 5.8 nm	No significant cytotoxicity	Ultrasound imaging-guided tumor photodynamic therapy

Author Manuscript Author Manuscript Author Manuscript Author Manuscript

Table 2.

Summary of inorganic nanosized UCAs for ultrasound imaging applications.

Inorganic nanoparticles	Composition	Size	Cytotoxicity	Applications
Silica NPs [55]	Solid spheres	330 nm in diameter	No acute toxicity	Targetable contrast agent for ultrasound imaging
Hollow silica NPs [56]	Surface PEGylated hollow silica microspheres	~1250 nm in diameter	Low cytotoxicity	Ultrasound contrast agents for imaging
Hollow hard porous silica NPs [57]	Hollow hard porous silica shell; filled with perfluorocarbon gas	2 μm in diameter; 10 nm thick porous silica shell	Low cytotoxicity	Tumor imaging
Mesoporous silica NPs [58]	Mesoporous structure	Pore diameter 2.4 nm; pore volume 0.98 cm^2.	Tumor-specific cytotoxicity	US-based breast cancer imaging
Mesoporous silica NPs [59]	Superhydrophobicity	Pore diameter < 1 nm	N/A	Targeting ultrasound imaging
Rattle-type mesoporous silica NPs [60]	Nanorattle hollow structure	NP diameter 420 nm; core diameter 260 nm	No evident toxicities	Intracellular ultrasound molecular imaging
Exosome-like silica NPs [61]	Concave mesoporous structure	140 nm in diameter	No detectable toxicity	Stem cells imaging and drug delivery
Fe-doped hollow silica nanoshells [62]	Ultrathin nanoshells with varying shell thicknesses and fused nanoflakes	2.4–22.8 nm in diameter; nanoflakes thicknesses 1.4–3.8 nm;	Minimal toxicity	Long-imaging capability for tumor
Au-PLGA NPs [63]	PLGA shell and perfluorohexane liquid core	200 nm in diameter	No detectable toxicity	Contrast-enhanced US imaging
Au-nanoshelled PLA nanocapsules [64]	Perfluorooctylbromide and superparamagnetic iron oxide nanoparticles coloading	300.4 nm in diameter	No evident toxicity	Contrast imaging-guided photothermal therapy
MnO_2 NPs [54]	Catalytic property	180 nm in diameter	No significant cytotoxicity	Tumor photodynamic therapy
Albumin-MnO_2 NPs [65]	Polyelectrolyte-albumin complex and MnO2 nanoparticles	~50 nm in diameter	Low cytotoxicity	Treatment of cancer
CO_2-generating $CaCO_3$ NPs [52]	Doxorubicin-loaded calcium carbonate hybrid nanoparticles	Mean diameter 145.2 to 240.8 nm	No appreciable toxicity	US imaging and simultaneous therapy of tumors
Prussian Blue NPs [66]	Catalytic property	Mean diameter 126.7 nm	No acute toxicity	Contrast-enhanced US imaging
Hollow mesoporous Prussian Blue nanocubes [67]	Hollow mesoporous Prussian Blue shell and perfluoropentane core	500 nm	No observable toxicity	US imaging-guided tumor detection and therapy
Superparamagnetic hollow Fe_3O_4 NPs [43]	Perfluorohexane-encapsulated hollow nanoparticles	Average particle size 537.3 nm	No distinct cytotoxicity	Stimuli-responsive cancer theranostics
Multiwalled carbon nanotubes [68]	Oxidized and functionalized to make them biocompatible (ox-MWCNT-NH_3^+)	Diameter 20–30 nm; Mean length 400 nm	No detectable toxicity	Contrast-enhanced US imaging
Multiwalled carbon nanotubes [69]	Antibody modification	Mean length ~150 nm	Negligible cytotoxicity	Targeted US imaging of tumor

Author Manuscript

Author Manuscript

Author Manuscript

Author Manuscript

Table 3.

Organic and inorganic nanosized contrast agents reported in the literatures for PA imaging applications.

Organic nanomaterials	Small organic molecules	Cyanine-based dyes, croconine, naphthalocyanines, perylene-diimide (PDI), phthalocyanine, porphyrin, porphysome, squaraine
	Semiconducting polymer NPs	semiconducting polymers, PDI-based NPs, organic NPs, oligomers, chlorin dimers, polypyrrole, polylysine, natural humic-acid-based nanoagents
Inorganic nanomaterials	Metallic NPs	Gold NPs, gold NP assemblies, Prussian blue, copper neodecanoate NPs, Ag NPs, Pd nanosheets
	Transition metal chalcogenides/ MXene-based NPs	CuS, Ag_2S, CulnS/ZnS, MoS_2, TiS_2, WS_2, CoS_2, ReS_2, Bi_2S_3, $MoSe_2$, Nb_2C, TaC, Ti_3C_2, S_2V
	Carbon-based NPs	Au coated SWCNTs, single-walled carbon nanotubes (SWCNTs)-Arg-Gly-Asp (RGD) conjugation, rGO loaded AuNR, rGO loaded AuNRVe, CNTR@AuNPs
	Others	Te nanosheets, B nanosheets, Cu-Ag_2S NPs, black-phosphorus quantum dots, black-phosphorus nanosheets, Fe@γ-Fe_2O_3@H-TiO_2 nanocomposites, MnO_x loaded Ti_3C_2

Author Manuscript Author Manuscript Author Manuscript Author Manuscript

Table 4.

Summary of PA imaging applications using different nanosized contrast agents.

Application	Nanosized UCA	Features	Performance
Deep tumor imaging [98]	Micelle enveloped PDI NPs	High PA imaging sensitivity, high photostability and biocompatibility	The NPs provided high PA imaging contrast for detection of deep brain tumor in living mice.
Brain tumor imaging [99]	Second NIR (NIR II) conjugated polymer NPs	High imaging contrast, high photostability and good biocompatibility	The NPs showed much weakened light attenuation, strong signal/background ratio, and large penetration depth for brain tumor imaging.
Brain vascular imaging [100]	Conjugated polymer nanoparticles (CPNs)	High photostability, exhibiting no toxicities both in vitro and in vivo	The NPs can greatly enhance PA signals for brain vascular imaging.
Deep brain glioma imaging [101]	MoS_2-ICG hybrid	High PA imaging sensitivity, enhanced photoacoustic conversion efficiency compared with ICG	Brain tumor at twofold deeper site beneath a mouse scalp was clearly identified by using the hybrid as contrast agent.
Mouse brain imaging [102]	ICG - containing porous Si NPs	ICG sealed within a rigid NP that can protect the ICG payload from thermal and photolytic degradation	The PA efficiency was increased 17-fold compared with free ICG.
Vessel atherosclerosis imaging [103]	ICG@PEG-Ag_2S nanoprobe	Long blood circulation, hemocompatibility, and no organ toxicity	Atherosclerotic plaques were imaged in a high contrast-enhanced manner.
Venous thrombosis imaging and antithrombotic therapy [104]	Thrombus-specific theranostic NPs	H_2O_2-triggered photoacoustic signal amplification	Photoacoustic contrast was greatly enhanced by using the NPs as contrast agent in a thrombosed vessel.
Venous thrombosis imaging [105]	cRGD peptide modified PDI NPs	High PA intensity, high photostability and biocompatibility, and excellent binding ability with GPIIb/IIIa	The PA contrast enhanced by the NPs provided effective information about the thrombus including the profile, size, and spatial distribution.
Sentinel lymph node (SLN) imaging [106]	Silica-coated gold nanoplates	High photothermal stability, and low cytotoxicity	Strong and sustained PA signals were obtained for SLN imaging in a mouse model.
Lymph node imaging in living mice [107]	Semiconducting polymer nanoparticles	High structural flexibility, high photostability, and narrow photoacoustic spectral profiles	They can not only be utilized for LN mapping but also for PA imaging of ROS.
Sentinel lymph node imaging [108]	Encapsulated conjugated oligomer NPs	Excellent photostability and biocompatibility, strong absorption in the NIR range	The NPs showed great potential for SLN imaging and photothermal therapy.
Detection of cancer-related matrix metalloproteinases [109]	Copper sulfide NPs	Strong absorbance in the NIR range, good photostability	The NPs could dramatically improve the tissue penetration depth for PA imaging.
Tumor hypoxia imaging [110]	Ratiometric hypoxia probe 1 (rHyP-1)	Strong NIR absorption, and deep penetration depth	The probe enabled high resolution hypoxia detection using PA imaging at centimeter depths.
Tumor pH imaging [111]	pH - responsive albumin - based nanoprobe	High biocompatibility, easy to operate, and depth independent accuracy	The nanoprobe was clinically adoptable for real-time pH imaging of the whole tumor.
pH imaging [112]	Semiconducting oligomer NPs	Ultrasmall size, high stability, and high pH sensitivity	The NPs allowed real-time PA imaging of pH in tumors in living mice.
Lithium detection [113]	Lithium ionophore	Monitoring therapeutic drug concentrations in vivo based on PA imaging	To track the concentrations of therapeutic drugs and improve disease management.
Methylmercury ($MeHg^+$) detection [114]	Liposome (LP) and cyanine dye (hCy7) nanoprobe	The hydrophobic hCy7 was encapsulated in the lipid layer of the liposome.	The nanoprobe can detect $MeHg^+$ in vivo by ratiometric photoacoustic bioimaging.

Application	Nanosized UCA	Features	Performance
		High biocompatibility and negligible cytotoxicity	

Author Manuscript
Author Manuscript
Author Manuscript
Author Manuscript